10

Vacuum Electron Sources and their Materials and Technologies

G. Gaertner and H.W.P. Koops

10.1 Thermionic Vacuum Electron Sources

10.1.1 Historical Development

Since the discovery of cathode rays in 1859 by Prof. Julius Plücker in Bonn [1] in the so-called Geißler tubes, manufactured by the skilled German mechanic Heinrich Geißler in Bonn since 1854, who had also developed an improved mercury vacuum pump, cathode ray based tubes have contributed a major part to the technological progress of the western world in the next 150 years to come. Cathode rays are nothing else than electron beams, and it lasted another 32 years since George J. Stoney from the UK introduced the term electron [1]. Usually only the name of T.A. Edison from the USA is known to the broader public, who started to sell incandescent light bulbs for 50 cents in 1883. Yet he had only developed this bulb in parallel to Joseph W. Swan from the UK, who introduced an incandescent lamp with a carbonized bamboo fiber as heated filament and an extraordinary long life of 40 hours in 1878. Edison had already experimented with a lot of different electrode materials, besides carbon-based materials also with Pt, Ir, Ba, Rh, Ru, Ti and Zr, but with limited success. But in the year 1883 T.A. Edison also showed that a current is flowing from the glowing cathode to the anode in a vacuum tube [1].

Typically vacuum electron tubes consist of an electron source, a vacuum or low pressure region where the extracted electrons interact with electric fields of either dc or ac/rf nature (e.g. defined by several grids or metal boundaries at certain applied potentials) and the collector or anode where the electrons are collected and continue to flow into a solid conductor. Our main interest in this chapter will be focused on the emission mechanisms and the different types of electron sources.

Regarding electron emission capabilities as a function of time (Fig. 10.1), there has been a continuous improvement [2, 3]. This was by part triggered by material systems change, partly by improved structural design and in the last two decades by

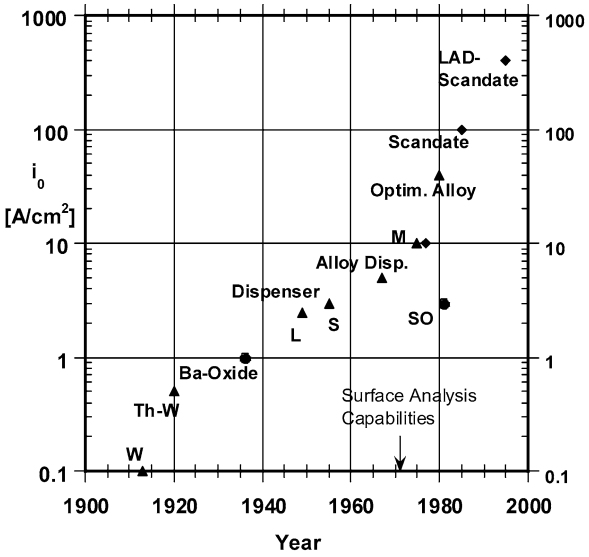

Fig. 10.1. Historical development of thermionic cathodes emission capabilities (life t_{op} at saturated emission current density ≥4000 h) [7]

increased contribution of sub-μm scale technologies, accompanied by high resolution characterization. The emission current densities given in Fig. 10.1 are related to a cathode life ≥4000 h. Of course, the introduction of new cathodes was also linked to certain tube applications.

In 1898 the Austrian Carl Auer von Welsbach introduced osmium wire as electrode in an incandescent light bulb, thus improving the usable life. In 1908 William David Coolidge from the USA found a method to draw thin tungsten wires and equipped incandescent light bulbs with heated tungsten wire coils [1]. Such tungsten filaments are used up till nowadays in X-ray tubes as cathodes due to their rather high insensitivity against gas poisoning and ion bombardment. Yet their emission current density at an operating temperature of about 2600°C is rather low, about 1 A/cm^2.

The oxide cathode was discovered by Arthur Rudolf Wehnelt in 1903 [4], who found that Geißler tubes equipped with such a cathode consisting of alkaline earth oxides could be used as current rectifiers. Since then the oxide cathode has been subject of extensive scientific studies and has become of great technological importance. Curiously enough, this stems from the art of making and utilizing it and not from a thorough understanding of the cathode. Development and improvement was in part guided by the contemporary physical models, which failed in other aspects later on or turned out to be incomplete [5]. In the years before World War II, the predominant view was (e.g. Reimann 1934 [6]) that Ba on the oxide surface, which was supplied by the interface reaction via diffusion, determined electron emission.

Part of the past and present improvements of vacuum electron tubes were made possible by improved cathodes [3]. Especially in the last 50 years Philips, as one

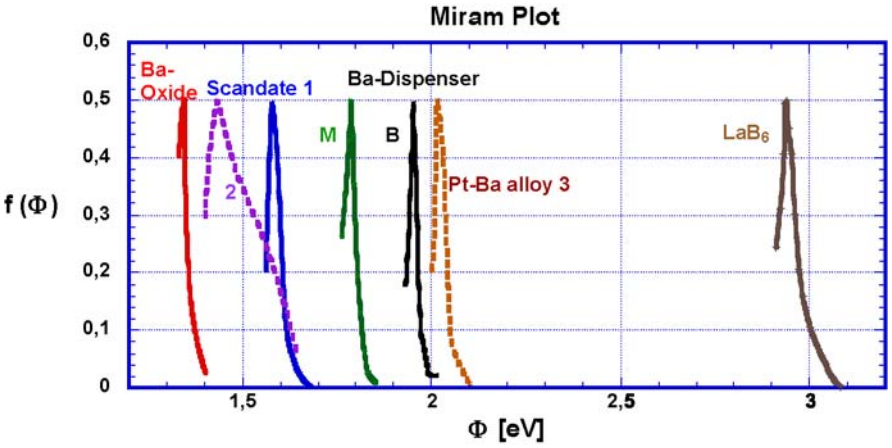

Fig. 10.2. Practical work function distributions (PWFD) or Miram plots, based on underheating or roll-off curves, of "best of class" thermionic cathodes [8]. Data are from Varian except *1* Deckers (mixed matrix scandate: Philips, The Netherlands), *2* Gaertner (LAD top-layer scandate: Philips, Germany) and *3* Djubua (Istok, Russia)

of the major vacuum tube manufacturing companies, was always at the top of innovation in the cathode field, as can be seen from the invention of the L-cathode in 1949 by Lemmens et al. and of the first impregnated Ba-dispenser (or I-) cathodes by Levi in 1955. In 1966 then Zalm et al. introduced the so-called M (magic) cathode with an Os/Ru top-layer on a 411 impregnated tungsten base. In 1995/97 G. Gaertner et al. improved the emission capability of Scandate cathodes from 120 A/cm^2 to 400 A/cm^2 at a true temperature of 1030°C (Os/Ru-I: 15 A/cm^2), which still represents world record in thermionic emission [7]. In a historical review Fig. 10.1 shows the development of the emission capabilities of thermionic cathodes in the last century (life end at saturated emission current density $\geq$4000 h). In Fig. 10.2 practical work function distributions (PWFD) or Miram plots based on underheating or roll-off curves are shown for "best of class" thermionic cathodes [8]. The LAD top-layer Scandate cathode peak (2) is situated at 1.43 eV near the oxide cathode peak.

In the following contribution a review of the basics and of present research and development activities on thermionic cathodes for vacuum tubes is given and also the progress in other emitters and the specific application advantages of the different cathode types are commented. Besides basic investigations of I cathodes and Scandate cathodes also improvements of oxide cathodes are addressed in more detail.

10.1.2 Fundamentals of Thermionic Emission

The basic equations governing thermionic emission or thermal electron emission can be derived straightforward for metals, where the energy levels are occupied up to the Fermi level E_F, which in this case lies in the conduction band. If the metal is heated to a temperature T, some of the electrons in the conduction band acquire sufficient

energy $> E_{\min}$ in order to reach the vacuum level and escape from the metal,

$$E_{\min} = E_{\mathrm{F}} + e\Phi, \tag{10.1}$$

where $e\Phi$ is the work function (Austrittsarbeit).

We can now calculate the density of electron gas in a short distance in front of the metal surface when in equilibrium with the emitter and also the number of electrons crossing a plane (cathode surface A) in this distance at time t_0 in both directions. Under saturation conditions all electrons of sufficient energy leave the cathode, with exception of a small fraction reflected at the surface represented by the reflection coefficient. A detailed derivation can be found in "Moderne Vacuumelektronik" by J. Eichmeier, pages 59–63 [9] and also in some other standard textbooks and review articles on thermionic emission [10, 11, 14, 15].

The differential density $\mathrm{d}N$ of electrons in the velocity interval between $v_{x,y,z}$ and $v_{x,y,z} + \mathrm{d}v_{x,y,z}$ is given by

$$\mathrm{d}N = 2v_x A t_0 m_{\mathrm{e}}^3/h^3 * (1/(1 + \exp((E - e\Phi)/kT))\,\mathrm{d}v_x\,\mathrm{d}v_y\,\mathrm{d}v_z, \tag{10.2}$$

where $E = m_{\mathrm{e}}(v_x^2 + v_y^2 + v_z^2)/2$. The differential emission current density belonging to $\mathrm{d}N$ then is given by

$$\mathrm{d}j_{\mathrm{s}} = e\mathrm{d}N/(At_0). \tag{10.3}$$

By integration of $\mathrm{d}j_{\mathrm{s}}$ from $v_{x,\min}$ to ∞, j_{s} can be obtained, also taking $E \gg E_{\mathrm{F}}$ into account for emitted electrons

$$j_{\mathrm{s}} = \int \mathrm{d}j_{\mathrm{s}} = \int \frac{e\,\mathrm{d}N}{t_0 A} = \frac{2em^3}{h^3}\mathrm{e}^{E_{\mathrm{F}}/kT}\int_{v_{x,\min}}^{+\infty}\int_{-\infty}^{+\infty}\int_{-\infty}^{+\infty} v_x \mathrm{e}^{-\frac{m}{2kT}(v_x^2+v_y^2+v_z^2)}\,\mathrm{d}v_x\,\mathrm{d}v_y\,\mathrm{d}v_z. \tag{10.4}$$

Integration then yields the equation

$$j_{\mathrm{s}} = 4\pi emk^2T^2/h^3 * \exp(E_{\mathrm{F}}/kT) * \exp\bigl(-mv_{x,\min}^2/2kT\bigr), \tag{10.5}$$

which is known as the Richardson–Dushman equation. It is usually written in the form

$$j_{\mathrm{s}} = A_{\mathrm{R}}T^2\exp(-e\Phi/kT), \tag{10.6}$$

where A_{R} is the Richardson (or better thermionic) constant, since the term Richardson constant is often used also for phenomenological values different from 120.4 $\mathrm{A\,cm^{-2}\,K^{-2}}$, and $e\Phi$ is the work function. Both constants can be determined from the I/U emission characteristic, where j_{s} is the point of deviation from the space charge limit, via a Richardson plot of $\ln(j_{\mathrm{s}}/T^2)$ versus $1/T$.

Of course, the validity of this equation is limited to ideal cases of metals with uniform surface and zero extraction field at the surface, which in reality is only obtained if the space charge field of the electron cloud in front of the surface is compensated by the external extraction field, i.e. the Laplace field between cathode and anode. Hence saturated thermionic emission is also called zero field thermionic emission. If the fixed thermionic constant is used in a Richardson plot instead of a fitted constant A_{R}, a temperature dependent term in the work function is obtained. Usually, due to the variations in A_{R}, this term is much larger than the theoretical estimation, which is of the order of k/e [11].

The equation can also be applied at very low current densities (e.g. at very low temperatures below the usual operating temperatures), but here in the generally called retarding field region with retarding potential U_a also the contact potential between cathode and anode (= difference between cathode and anode work function $= e\Phi_K - e\Phi_A$; order of magnitude 1 eV) has to be taken into account. The emission current density j_a is then given by

$$j_a = j_s \exp\{(-eU_a + (e\Phi_K - e\Phi_A))/kT\}. \tag{10.7}$$

Using the thermionic cathode at intermediate current densities up to saturation, a space charge limited emission is obtained (virtual cathode at space charge maximum at distance d_m). Here the space charge limited current I_{SCL} is practically independent of the temperature, but depends on the field strength U_a/D in front of the cathode,

$$I_{SCL} = (4/9)\varepsilon_0\sqrt{2e/m_e}(A_k/D^2)U_a^{3/2} = KU_a^{3/2}. \tag{10.8}$$

The geometry factor $K = 2.33 \times 10^{-6} A_k/D^2$ is given in units of $A/V^{3/2}$, where A_k is the emitting cathode surface area, D the cathode to anode distance and U_a the anode voltage in V. Further corrections of space-charge limited emission arise by taking the electron velocity distribution into account; U_a then has to be replaced by the difference of $U_a - U_m$, where U_m is the threshold potential and D_m the distance of the space charge maximum. The equation for I_{SCL} is then modified to [9]

$$I_{SCL} = (4/9)\varepsilon_0\sqrt{2e/m_e}A_k(U_a - U_m)^{3/2}/(D - D_m)^2 * \{1 + 2.66\sqrt{(kT/(eU_a - eU_m))}\}. \tag{10.9}$$

Also in the saturation range a further slight increase of current density with increasing field strength can be observed. This is due to the mirror image charge and is called Schottky effect in honour of Walter Schottky, who first derived it. Extracting the saturation current using an accordingly high anode voltage U_a, e.g. in a diode configuration, reduces the work function slightly by the high field strength E_k at the cathode. The Schottky effect can result in an increase of the saturation current of up to 10% or more. The resulting saturation current density in most cases can be measured in pulsed operation only, due to the high power load on the anode.

The superposition of the $1/r$ potential of the mirror image charge with the Laplace electric field as shown in Fig. 10.3 leads to a reduction of the potential maximum in front of the cathode by

$$\Delta U_k = \sqrt{((eE)/(4\pi\varepsilon_0))}. \tag{10.10}$$

This then implies further modification of the Richardson–Dushman equation by inclusion of this field dependent decrease of the work function [9], where E is given in V/cm and T in K,

$$j_s = A_R T^2 \exp(-e\Phi/kT) \exp\left(4.4E^{1/2}/T\right). \tag{10.11}$$

It has to be pointed out that this equation has to be modified further, since space charge, of course, is also present in the accelerating field range and hence the Laplace

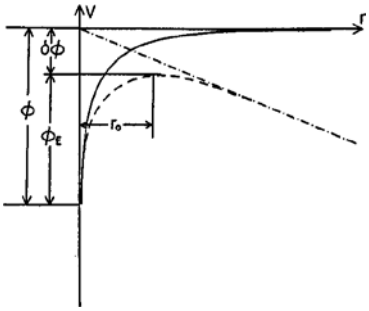

Fig. 10.3. The effect of an accelerating electric field on the work function of a metal: image potential (—); potential due to the applied electric (Laplace) field (-·-·-); and total potential (- - - -) [12]

field is modified by the space charge. A complete theoretical description of this range is given by Scott (numerical approach) and Hasker [13], where Hasker deduced an approximate theory in closed form.

Another reduction of a clean metal work function can be caused by adsorption of an electropositive monolayer. This subtractive dipole moment of the adsorbed atoms reduces the work function by $4\pi ned$, where n is the density of adsorbed atoms per cm^2, e is the electron charge and d is the dipole distance, typically of the order of 0.1 nm. Of course, adsorption of an electronegative monolayer will then lead to a similar increase of the work function [16].

When an electron leaves the cathode surface, it takes with it an average kinetic energy of the amount $2kT$. Also, since the electrons that must replace it are at the Fermi level on average, an additional amount of energy $e\Phi$ is required to raise an electron to the vacuum level. This electron emission cooling effect was first derived theoretically by O.W. Richardson in 1903 and is used for a calorimetric determination of the work function [14].

For high emission currents the cooling effect partly compensates cathode heating (e.g. via resistive or radiative heating) and leads to a current dependent temperature decrease of the cathode. This cooling can become noticeable at operating temperatures and sufficiently high dc-emission currents. For pulsed currents the duty cycle has to be taken into account. In a planar configuration the cooling power ΔP_{cool} is proportional to the the emission current I_{e} and to the average energy uptake of the electrons leaving the cathode according to [15, 19], being valid for the space charge and for the Schottky region:

$$\Delta P_{\mathrm{cool}} = I_{\mathrm{e}}(\Phi + kT/e * \ln(I_{\mathrm{s}}/I_{\mathrm{e}}) + 2kT/e), \tag{10.12}$$

where T is the true temperature. For a cylindrical configuration $2kT/e$ has to be replaced by $5kT/2e$. In case of $I_{\mathrm{s}} = I_{\mathrm{e}}$ the case of onset of saturation or zero field emission I_{s} is obtained:

$$\Delta P_{\mathrm{cool}}(\mathrm{sat}) = I_{\mathrm{s}}(\Phi + 2kT/e). \tag{10.13}$$

The contribution of the Thomson effect usually is negligible. The term with $\ln(I_s/I_e)$ for $I_e > I_s$ also takes the work function decrease due to the Schottky effect in the accelerating field range into account. The cooling of the cathode can be evaluated from the $T(P)$ diagram, where temperature T[K] versus heating power P[W] is plotted. The change in temperature T by $-\Delta T$ (in the ordinate) by emission cooling corresponds to a change in power P by $-\Delta P_{cool}$ (in the abscissa).

10.1.3 Types of Thermionic Cathodes, Properties and Applications

Metal Cathodes

In order to be useful as a cathode, a clean metal must give sufficient emission current density at a temperature where it does not evaporate too rapidly. As a rough guide vapour pressures in the range 10^{-7} to 10^{-9} mbar can be regarded tolerable for most purposes. This limits the choice to a few metals such as W, Re or Ta with a high melting point, which usually belong to the refractory metals and are not so easily machineable, especially tungsten [6].

This choice is substantiated by the following Table 10.1, where melting points and work functions of metals/elements used in vacuum electronics are listed. It is taken from Jenkins [16], with some additions. It has to be noted that to a good approximation the metal work function can be estimated by the image force Coulomb potential at the metal atomic radius: $e\Phi = e^2/(8\pi\varepsilon_0 r)$.

W, Ta and Re have the advantages that due to their high operating temperature contaminating electronegative gases are rapidly evaporated, and thus they are able to emit satisfactorily in poor vacua needing only a small temperature increase to suppress poisoning. For this reason tungsten is generally used in ionization gauges, high power electron guns for electron beam welding and in unbaked demountable systems. The disadvantages are that it needs a high amount of heating power (70 W cm^{-2} at 2500 K), is also subject to a reversible reaction with water vapour and can form

Table 10.1. Usable electron emission from clean metals/elements

Metal	MP (K)	T (K) for $p_{vap} = 1.3 \times 10^{-7}$ mb	A_R (A cm^{-2} K^{-2})	$e\Phi$ (eV)	j_s (A cm^{-2})
W	3640	2520	80	4.54	0.4
Ta	3270	2370	60	4.10	0.6
Re	3440	2330	700	4.7	0.26
Mo	2890	1970	55	4.15	5×10^{-3}
Os	2973	2310	120.4	5.5	6.4×10^{-4}
Ir	2727	1770	120.4	5.4	1.6×10^{-7}
C	4400	2030	48	4.35	2×10^{-3}
Pt	2050	1650	170	5.40	2×10^{-8}
Ni	1730	1270	60	4.1	5×10^{-9}
Ba	1120	580	60	2.11	1×10^{-11}

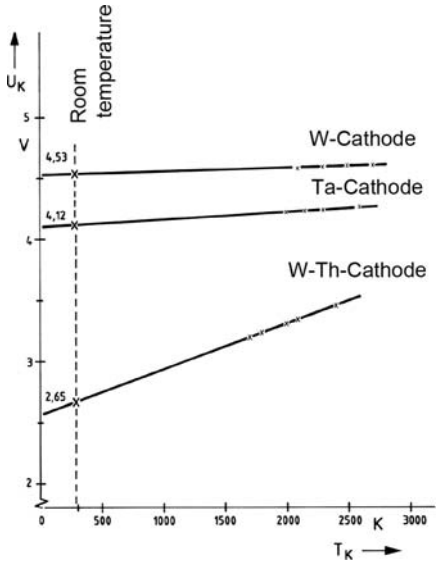

Fig. 10.4. Work function dependence on operation temperature for tungsten (W), tantalum (Ta), and thoriated tungsten (Th–W) wire cathodes [15]

tungsten oxides with oxygen in the rest gas, which may also react to CO with carbon containing contaminants. This is the reason why the more expensive Re or Ir are preferred in mass spectrometers for residual gas analysis.

For geometries other than wire usually Ta is preferred due to its high ductility and hence good machineability. It has the disadvantage that it is embrittled by hydrogen. Os, which was used at the beginning of the last century in incandescent lamps, has the disadvantage of forming a very volatile poisonous osmiumtetroxide with oxygen. The dependence of the work function on the operation temperature is shown in Fig. 10.4 for tungsten (W), tantalum (Ta), and thoriated tungsten (Th–W) wire cathodes.

Monolayer Thin Film on Metal Cathodes

The work function of pure metals can be lowered by a monolayer coating with a suitable element or dipole layer of two elements , as we have seen in the preceding paragraph. Of course, this layer can be provided from an external evaporation source of these elements, but usually this is impractical for long-life cathodes, who need a continuous resupply for compensation of the evaporation or ion bombardment induced loss of this film. Therefore, a reservoir, usually in the interior of the cathode, is needed where the monolayer elements are generated via a chemical reaction and migrate to the cathode surface, e.g. by grain boundary or pore diffusion. Such film cathodes are therefore also called dispenser cathodes [6].

Thoriated Tungsten Cathodes

By provision of an electropositive monolayer of Th on W, the work function of such a system $e\Phi = 2.7\,\text{eV}$ is by far lower than the work function of tungsten of 4.54 eV and even lower than that of Th of 3.5 eV [17].

The supply of Th is achieved by doping W with ThO_2 in form of small embedded grains and by carburization of a top layer of tungsten, e.g. to one third of the W wire diameter. After activation and during life, free Th is then generated via the reaction between thoria and tungsten carbide:

$$2\,W_2C + ThO_2 \rightarrow 4W + 2\,CO + Th. \tag{10.14}$$

Th is migrating to the surface via grain boundary diffusion and spreads on the surface via surface diffusion [16].

Thus, much higher current densities at much lower wire temperatures can be provided by thoriated tungsten cathodes (see Fig. 10.5). The typical operating temperature is 2000 K, where the Th–W cathodes can provide a saturated emission of

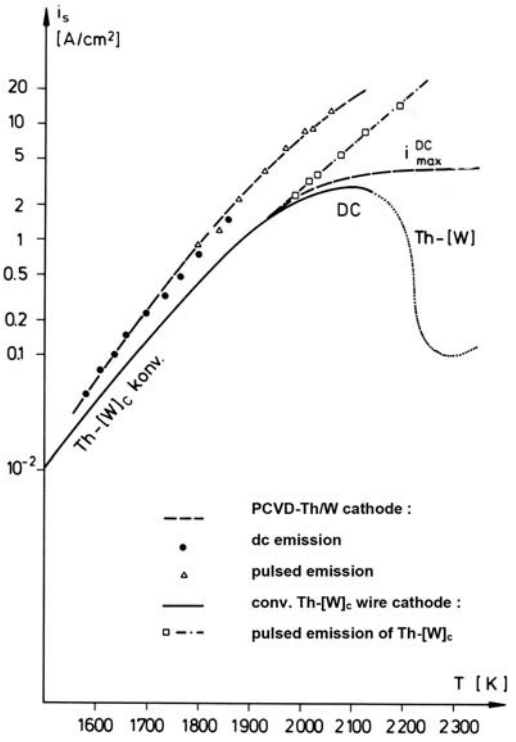

Fig. 10.5. Saturated emission current density as a function of temperature for thoriated tungsten: conventional carburized thoriated tungsten wires were measured in a cylindrical diode. Samples of Th/W cathodes manufactured by plasma-activated CVD were measured in a planar diode configuration [20, 21]

4 A cm^{-2} with a life in excess of 10 000 h. The Th–W cathodes are typically applied in rf tubes such as tetrodes or magnetrons used for rf/radio transmission and rf heating. The thoriated tungsten wires are either assembled into a "squirrel cage" or with an open basket weave, and are directly heated. The valves usually contain Zr heated by radiation from the cathode to act as a getter for the oxidizing gases.

In 1987 G. Gaertner et al. succeeded in providing unipotential cylinder cathodes of thoriated tungsten by plasma-activated CVD from a reactive gas phase containing WF_6/H_2 and Th-β-diketonate starting compounds [21]. There exists a lot of variants of thoriated cathodes, e.g. characterized by replacement of W by Re, Os, Ta at least at the surface or by surface layers with preferential crystal orientation, as pioneered by Ira Weisman [18] for W. Carburization can also be replaced by boriding, e.g. with the aid of diborane, then obtaining a borided tungsten cathode. Also improvements in emission can be achieved by addition of the so-called mobilizers such as Pt, Zr, Hf, Al , Ta enhancing grain boundary diffusion [22].

Lanthanated Molybdenum Cathodes

Replacing thorium by lanthanum and tungsten by molybdenum the lanthanated Mo cathode or LM cathode is obtained, which was introduced and investigated by C. Buxbaum et al. of BBC in the years 1976–1980 [22].

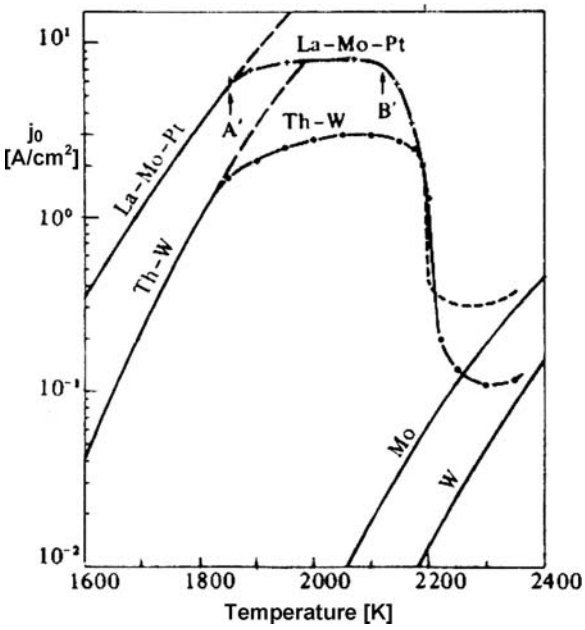

Fig. 10.6. Emission current density of La–Mo–Pt sintered cathodes as a function of temperature. At point A′La evaporation becomes dominating over diffusional supply. Thoriated tungsten, Mo and W are depicted for comparison [22]

The advantage over Th–W cathodes are lower operating temperatures for comparable emission current densities. Thus, in the range 1780–1900 K the LM cathode can deliver 3.5–8 A/cm^2 (see Fig. 10.6). These cathodes are rather insensitive to gas poisoning and can be completely reactivated after venting the chamber or tube. Mo is also easily machineable. The typical dopant amount of La_2O_3 in Mo is 1–4% by weight, the optimum being about 2%. Mo is carburized similar to tungsten. It is also advantageous to coat the surface with a 0.2–10 µm thin Pt layer, where La has a higher sticking coefficient, i.e. the cathode can be stably operated at somewhat higher temperature.

Ba-dispenser or I-cathodes

For high end television tube applications Philips in 1990 introduced Os/Ru coated impregnated (=I) cathodes, which show stable emission performance at 5–10 A/cm^2 up to 25 000 h [23, 27]. Here the cathode base consists of porous tungsten with about 20% porosity, impregnated with $4BaO{\cdot}CaO{\cdot}Al_2O_3$ (=411). The use of osmium
coated and uncoated Ba-dispenser cathodes was a breakthrough with respect to loadability and low temperature film cathode operation. A predecessor of the I cathode was the metal capillary cathode (Siemens designation MK cathode) or reservoir cathode (Philips designation L-cathode), where a reservoir containing a.o. BaO is situated behind a porous tungsten plug [16]. A recent version of it is described by B. Vancil [25]. Figure 10.7 presents the work function dependence on the operation temperature for osmium coated and uncoated Ba-dispenser cathodes, especilly BaO reservoir cathodes. Despite their operating temperature being about 250°C higher than for oxide cathodes related to their higher work function (about 0.4 eV higher)

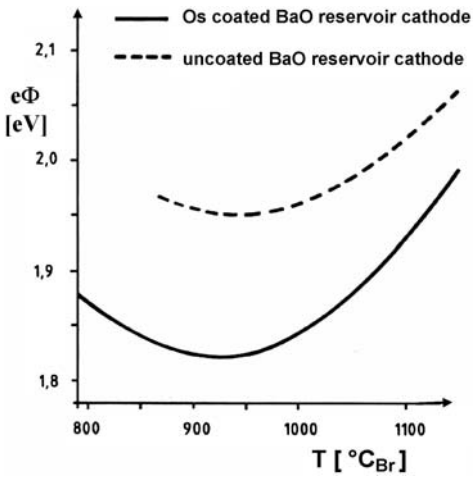

Fig. 10.7. Work function dependence on operation temperature for Osmium coated and uncoated Ba-dispenser cathodes [15]

and their higher production cost, they allow improved brightness and resolution of high end CRTs. The design of the 0.65 watt I-cathode units (see Figs. 10.8 and 10.9) is compatible with 0.65 watt oxide cathode units (see Fig. 10.14), so that they are exchangeable in the same tube type.

One of the important application issues is ion bombardment (IB) resistivity, since ions are created by electron impact on the rest gas. The IB behaviour of several Ba dispenser cathodes such as W-I, Re-I, Ir-I, Os/Ru-I and also Scandate-I was investigated in gun and diode configurations. In accelerated IB life tests at lower ion dose

Fig. 10.8. Philips 0.65 watt I cathode unit for CRTs

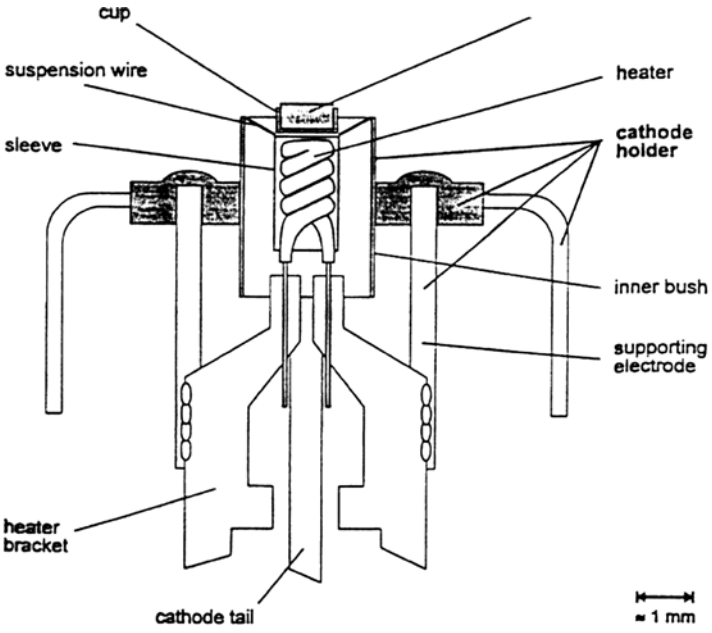

Fig. 10.9. Schematic cross-section of a Philips 0.65 watt I cathode unit

rates (see Fig. 10.11) a "dynamical shielding effect" [36] was observed due to continuous Ba resupply during IB, which improves extrapolation to realistic dose rates. In collaboration with TU Eindhoven, IB characterization was recently extended to more basic I-cathode surface investigations using low energy ion scattering (LEIS) and also Auger parallel to emission measurements [27]. Quantification of the results showed increased neutralization of the scattered Ar ions at I cathode surfaces the lower their work function. It was also observed that Ba will mainly reside on surface sites where oxygen is present in order to form a relatively stable Ba-O dipole layer. Hence IB recovery is also limited by presence and resupply of oxygen.

The highest Ba-O density is found for Os/Ru-I, which also has the lowest effective work function of all I-cathode types of about 1.8 eV. The concept of a fine-grained intermediate layer, in this case W, was also applied to Ir-I-cathodes by Toshiba [28], showing improved ion bombardment resistivity.

Ba-Scandate Dispenser Cathodes

Currently the most prominent thermionic cathode with respect to highest zero field emission current density i_0 is the Scandate cathode, despite the fact that high end applications are still dominated by advanced I-cathode types. The reason for this will be discussed later. Also, in Scandate cathode development a steady improvement of i_0 with time can be observed, linked to different types of Scandate cathodes. Starting with the pressed Scandate cathode, which is based on a patent of Figner in 1967, van Oostrom et al. [29] in 1979 realized $i_0 = 10\,\mathrm{A/cm^2}$ at $950°\mathrm{C_{Mo\text{-}Br}}$ operating temperature (1017°C true temperature). Comparable emission was achieved with the impregnated Scandate cathode invented by Philips (P. Zalm, A. van Stratum) in 1977, where Sc_2O_3 was added to the impregnant. Mixed matrix Scandate cathodes were first introduced by S. Yamamoto (Hitachi) in 1983 [30], where the matrix consisted of a mixture of tungsten and Sc_2O_3; J. Hasker (Philips) improved this in 1989 by using $W + ScH_3$ as a starting powder mixture [31, 32], yielding about $100\,\mathrm{A/cm^2}$ at the standard operating temperature. In 1984 J. Hasker had also pioneered the top-layer Scandate cathode, where a 5 µm layer on top of the porous W body, impregnated with BaCaAluminate, consisted of a mixed matrix of $W + Sc_2O_3$. Further variants of top-layer Scandate cathodes (in short, 'Sc'-I) were then introduced by sputter coating the W-base with $W + Sc_2O_3$(1986). Further improvement was found using $W + Sc_2W_3O_{12}$ (1989) [33] by S. Yamamoto et al. (Hitachi). In 1984 they also published results obtained with a combination of mixed matrix Scandate cathode with Ir, Os, Pt and Mo surface coating. U. van Slooten and P. Duine from Philips report increased ion bombardment resistivity of a Re-coated mixed matrix Scandate cathode in 1996 [34]. Top-layer (=T-L) Scandate cathodes prepared by plasma-activated CVD were investigated by G. Gaertner et al. [35], yielding $60\,\mathrm{A/cm^2}$ at $950°\mathrm{C_{Mo\text{-}Br}}$ in the best version. Currently besides the research activities of Philips and Hitachi on Scandate cathodes, also Hughes (sputtered T-L), Thomson, AEG, Samsung and other companies are active in this field.

To overcome disadvantages of the I cathode like high operating temperature (high Ba production!) and limited current density, Philips research realized a top-layer

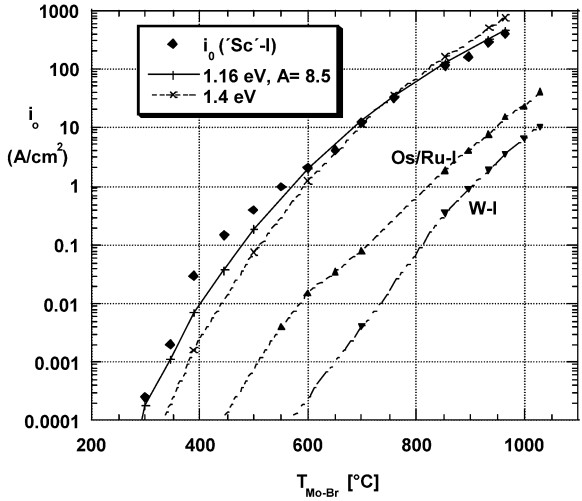

Fig. 10.10. Saturated emission current density i_0 as a function of temperature (Mo-brightness) for LAD top-layer Scandate cathodes ='Sc'/Re-I, Os/Ru-I and W-I cathodes. The *solid line* is the theoretical line for a Richardson work function of 1.16 eV and a Richardson constant of $A_R = 8.5\,\mathrm{A/cm^2\,K^2}$ [36]

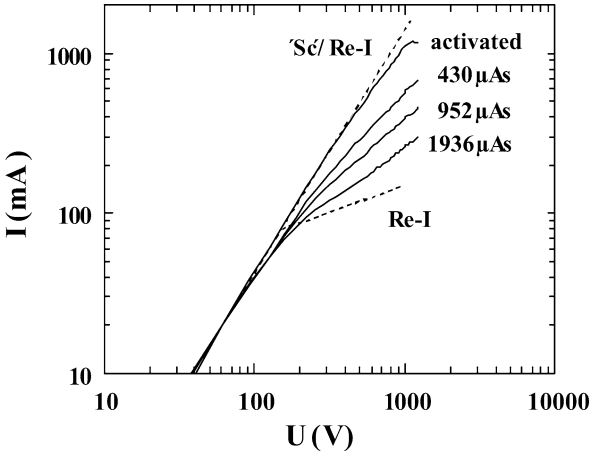

Fig. 10.11. Degradation of I/U characteristic as a function of IB dose: 10^4 µAs in diode @1 mA∗1 mbar∗s in electron gun; *dashed lines*: perfect 'Sc'/Re-I and Re-I cathodes; total emission is superposition of area fractions of scandate (only space charge limited) and Re-I [36]

Scandate cathode by laser ablation deposition (LAD), which is capable of unprecedented 400 A/cm^2 at the same operating true temperature as the I cathode of 1030°C [7, 36]. This allows a reduction of the 'Sc'/Re-I cathode operating temperature and also makes possible new high end applications. The top-layer Scandate cathodes

were prepared by Excimer-LAD of W/Re + Sc_2O_3 on 411 impregnated W-I cathode bases, usually already mounted in 0.65 W cathode units. The top layer of usually 100–500 nm thickness has a very fine grained structure prepared via nanoparticles [24], which is favorable for grain boundary and pore diffusion, a concept which has also been applied for other cathode types. The ion bombardment resistivity and also the emission uniformity of this cathode is strongly improved over previous scandate cathode types, which were either prepared by powder metallurgy or by sputter coating the top-layer. In order to illustrate also the exceptionally high emission of 'Sc'-I at low temperatures, in Fig. 10.10 the saturated emission current density i_0 is shown as a function of temperature (Mo-brightness) over the whole range from 200 to 1000°C for 'Sc'/Re-I, for Os/Ru-I and W-I cathodes [36]. The solid line is the theoretical line for a Richardson work function of 1.16 eV and a Richardson constant of $A_R = 8.5\ A\,cm^{-2}\,K^{-2}$, as determined from Richardson plot in the interval 600–1000°C. It gives a better fit to the experimental 'Sc'/Re-I data than an effective work function of 1.4 eV (with $A_R = 120.4\ A\,cm^{-2}\,K^{-2}$).

The measurements underline that the work function remains nearly constant over a wide temperature range. Also field emission with a low threshold of 3.2 V/μm has been observed for 'Sc'/Re-I. In the range from 250 to 350°C thermal assisted field emission is observed and the threshold vanishes [37]. Finally sputtered top-layer Scandate cathodes are investigated by Hitachi, Toshiba and by Y. Wang in China (see [23]) trying to improve them by variation of layer composition and structure. In one version Y. Wang and her group prepared a fine-grained mixed matrix Scandate cathode type with submicron matrix structure and improved emission behaviour [26].

Oxide Cathodes

Alkaline Earth Oxide Cathodes

Oxide cathodes are still lowest in cost. This is due to the rather cheap preparation method of spray coating (Ba,Sr,Ca)- or (Ba,Sr)-carbonate particles on a cathode Ni base. As a result a rather porous structure of about 75% porosity is obtained. Yet they are limited in dc current density to less than 3 A/cm^2. In 1986 Saito et al. from Mitsubishi [38] introduced scandia particle doping of the triple Ba·Sr·Ca-oxide coating in order to increase the critical dc current density $j_{crit,dc}$. P. Derks from Philips then in 1987/1992 replaced scandia finally by rare earth atomic doping of the oxides, especially using coprecipitated europia or yttria [22]. It was later shown by G. Gaertner et al. that the electrical conductivity and hence $j_{crit,dc}$ is increased proportionally to the coprecipitated rare earth addition, yet at the expense of increased oxygen poisoning sensitivity of the oxide cathode [40], if no additional measures are taken.

In Fig. 10.12 the effect of atomic doping with yttrium on conductivity is shown versus operation time. The comparison with the undoped cathode shows, that σ_{el} is increased over life. This was one of the reasons that now oxide cathodes doped with Ni particles are developed. The basic idea is to overcome the conductivity limitation by addition of acicular Ni particles, where 5% are already at the percolation threshold

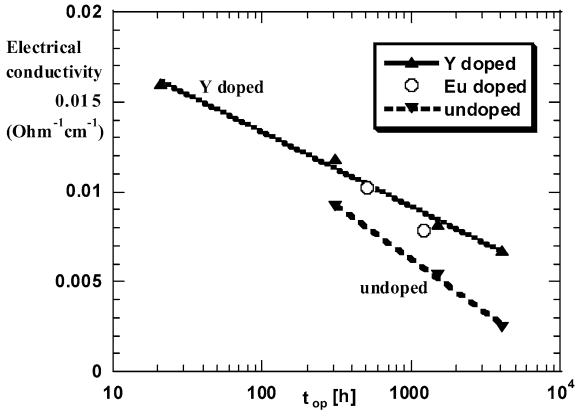

Fig. 10.12. Electrical conductivity σ_{el} of yttria doped and Eu doped Ba·Sr-oxide cathode compared to non-doped cathode versus operation time [40]

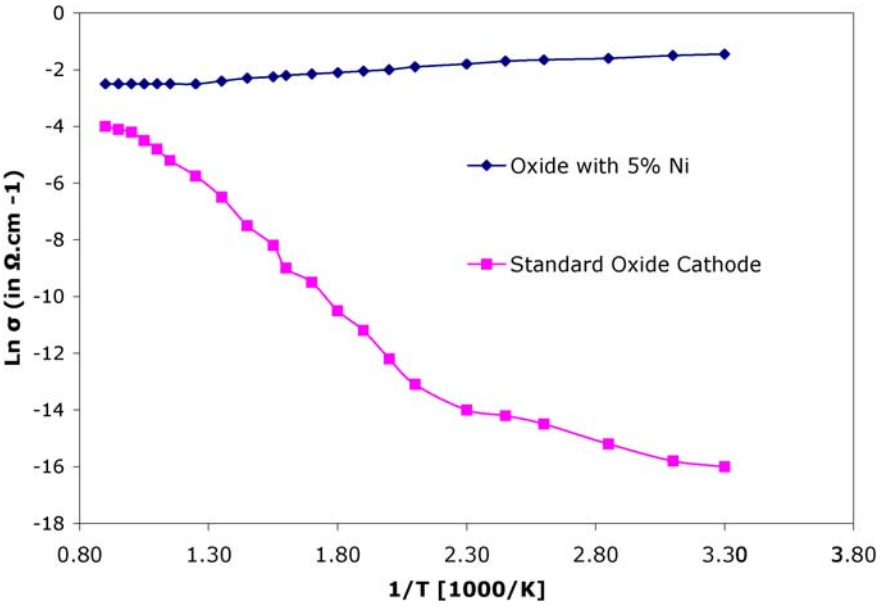

Fig. 10.13. Electrical conductivity versus reciprocal absolute temperature for Philips standard oxide and with 5% Ni particles added [41]

for metallic conduction. Conductivity measurements at the Sheffield–Hallam University for a 5% Ni doped cathode showed about 1×10^{-2} $(\Omega\,\mathrm{cm})^{-1}$ from 1000 K down to room temperature (see Fig. 10.13) [41], whereas oxide cathodes without Ni exhibit a strong conductivity decline with decreasing temperature. For 2.5% Ni addition $\sigma_{el} = 8 \times 10^{-3}$ $(\Omega\,\mathrm{cm})^{-1}$ was directly determined under operating conditions

Fig. 10.14. Philips 0.65 W oxide cathode unit for CRTs

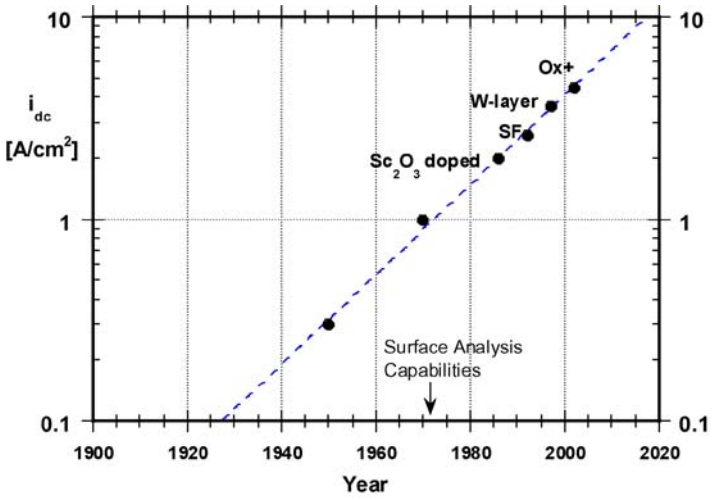

Fig. 10.15. Ba-Oxide cathode dc loadability improvement versus time (typical cathode life > 10 000 h)

at the (true) operating temperature of 1050 K in a planar diode, as described in [40]. Increased dc loadability at lower temperatures can be derived from Fig. 10.13.

As a further beneficial effect, the embedded nickel filaments have also been found to reduce the cut-off drift in CRT applications. This Ni addition is one of the distinctive features of the cermet Oxide Plus cathode of LG-Philips Displays (see Fig. 10.14) besides other improvements, which is able to deliver 3.5 A/cm^2 over life, with peak (dc) values up to 10 A/cm^2 [39]. The increase of the dc loadability of oxide cathodes as a function of time is shown in Fig. 10.15. Of course also a sufficient effort will be needed to continue with this progress in the future.

Improvements of Ba-oxide and Ba dispenser cathodes are also investigated by several other CRT companies and have been reviewed recently by e.g. Higuchi [42]. Therefore, we only want to give a short review of some promising developments. Besides numerous variations of the oxide additives started by Mitsubishi [38], one improvement option in oxide cathodes is the introduction of an additional layer at the interface. Here Samsung [43] introduced a fine-grained Ni top layer on the Ni base of about 1–2 μm thickness, which favors the activator diffusion along the grain boundaries to the oxide coating and implies increased Ba generation. These cathodes, additionally doped with Mg–La compound, can still be operated at 2 A/cm^2 after 12 000 h. Mitsubishi investigated a tungsten intermediate layer, but unfortunately delamination problems had to be overcome.

A further trend are much denser oxide cathodes, like the HIP cathode of NEC [23], where a mixture of Ni, Scandia and (Ba,Sr,Ca)-carbonate powders is pressed into a Ni–Cr container. Cr from the walls is playing the role of the activator. An emission life of 22 000 h at 3 A/cm^2 and 1153 K is claimed. Also, improvement is obtained by a much denser arc plasma deposited oxide cathode with respect to lower BaO evaporation and improved emission.

Other Oxide Cathodes: ThO_2

Thoria coated W, Ta or Ir filaments have been used in rf tubes and especially ThO_2 on Ir is still in use. They deliver current densities of about 5 A/cm^2 at 2000 K due to a low work function of 2.6 eV [93:502-503].

Boride cathodes: LaB_6, CeB_6

The thermionic emission properties of the borides of the alkaline-earth and rare-earth metals and thorium have been investigated in the 1950s [45]. These compounds all have the same formula MB_6 and the same crystal structure consisting of a three-dimensional boron framework in whose interlattice spaces the metal atoms are embedded. The valence electrons of the metal atoms are not accepted by the B_6 complex, thus giving rise to the presence of free electrons which impart a metallic character to these compounds. This, together with the strong bonds between the boron atoms in the framework, produces a series of compounds which have high electrical conductivities and high thermal and chemical stabilities, which are ideal properties for a cathode material. When this structure is heated to a sufficiently high temperature, the metal atoms at the surface evaporate. They are, however, immediately replaced by diffusion of metal atoms from the underlying cells. The boron framework does not evaporate but remains intact.

This process gives a mechanism for constantly maintaining an active cathode surface. Thermionic emission measurements made on these materials show the rare-earth metal borides to be superior to the others. The highest emission was obtained from lanthanum hexaboride, namely 6 A/cm^2 at 1600°C. Its emission constants for the Dushman equation were $e\Phi = 2.66$ eV and $A_R = 29$ A/(cm^2 K^2) [45]. This is higher than the emission normally obtained from thoria H. Ahmed and A. Broers in 1971 obtain [46] $e\Phi = 2.4$ eV and $A_R = 40$ A/(cm^2 K^2). Lanthanum boride has a

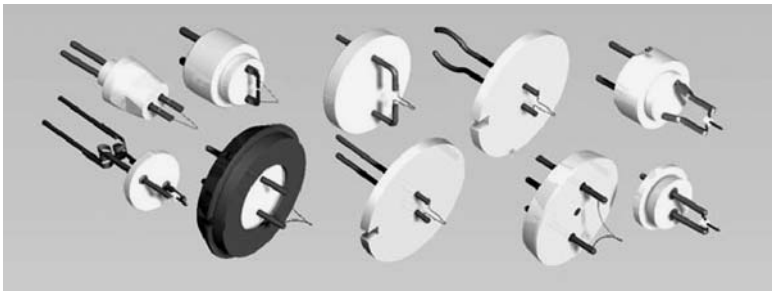

Fig. 10.16. Tungsten and boride cathode mounts for electron guns of many suppliers (courtesy of Kimball Physics [44])

relatively low evaporation rate corresponding to a latent heat of evaporation of 169 kilocalories per mole. If the hexaborides are operated at high temperature in contact with the refractory metals, boron diffuses into their metal lattices forming interstitial boron alloys with them. When this occurs, the boron framework which holds the alkaline-earth or rare-earth metal atoms collapses, permitting the latter to evaporate. However, the hexaboride cathodes may be operated at high temperatures in contact with tantalum carbide or graphite. Typical cathode mounts are shown in Fig. 10.16.

Lanthanum boride cathodes are especially useful in applications where high current densities and electron beams of high brightness are required. Despite these advantages they have a much higher operating temperature than Ba dispenser or Ba oxide cathodes. They are also suitable for high voltage applications because they stand up well under positive ion bombardment. Since they are atmospherically stable and activate easily, they have found wide use in experimental demountable systems.

LaB_6 cathodes use single crystal lanthanum hexaboride as emitter material, having a work function of 2.69 eV. The crystal with <100> orientation is mounted on a carbon heater rod, and held in place by a precision carbon ferrule. Special accuracy is employed to fabricate a round and smooth micro-flat at the top of the crystal of 1.7×10^{-6} cm^2 area. The heating current of 1.7 A to 2.1 A is delivered through a precision-machined, single-piece carbon rod with central slot and mounting strips. The ceramic sub-base provides rigidity and easier mounting. The Kimball Physics [44] ES-423E (extended life) lanthanum hexaboride cathode is a high performance, resistively heated, thermionic electron source, see Fig. 10.17. Guaranteed is a lifetime of thousands of hours in a clean vacuum system (UHV quality) at a pressure $<10^{-7}$ mbar. Operation at 20–30 A/cm^2 current density is recommended. The reactive lanthanum hexaboride crystal is clamped between or mounted in carbon. The temperature of the crystal is balanced to have high brightness of 10^7 A/(cm^2 sr), at a source size of 5 μm, and to have a low chemical evaporation rate of the crystal. This equilibrium is reached at a crystal temperature of 1700–1900 K. Due to the space charge limited emission from a surface at 1700 K the electron beam energy distribution has a low width of approximately 0.4 eV.

The small area of the heating current loop keeps the unwanted heater current magnetic field low. Because the rod is one single piece, no heating current passes

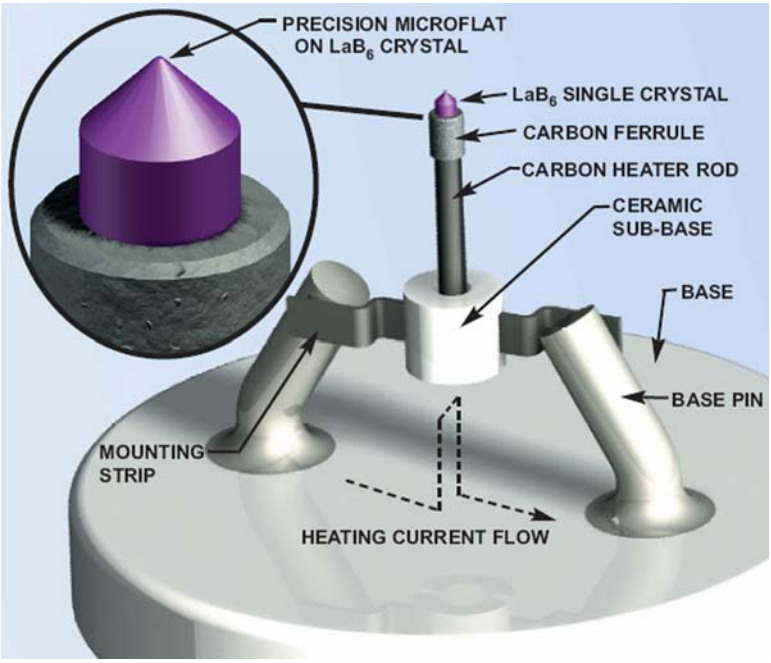

Fig. 10.17. Kimball Physics ES-423E (extended life) lanthanum hexaboride cathode [44]

through the crystal; there are no high temperature current-carrying joints. A high degree of axial symmetry keeps mechanical motions small. The small physical size fits most Wehnelts with ease. In the ES-423E, the crystal can be completely evaporated away without affecting the heating circuit. The very tight tolerances and the enclosed structure prevent the loss of LaB_6 in the mounting region throughout the entire crystal life. Reduced material loss also means less Wehnelt contamination.

In SEM type instruments, lifetimes up to 3000 to 4000 hours may be achieved at operating temperatures of 1850 K (corresponding to material surface loss rates in the 0.025 micron/hour range), with full brightness and excellent stability. With somewhat reduced brightness, as required by typical TEM instruments, lifetimes can be even longer. The ES-423E mounting structure will last more than 10 000 hours. Neither the electrical heating circuit drive impedance nor the thermal properties will drift perceptibly over that period. Chemical reactivity and mechanical drift problems have been eliminated. The real figure of merit of a thermionic electron emitter is the number of coulombs of electrons which may be boiled off per kilogram of cathode surface evaporated away. LaB_6 is an order of magnitude superior to the refractory metals in this key parameter. Any failure of a cathode mounting structure, before the LaB_6 cathode itself has been used up, represents a waste of cathode life. The ES-423E single-piece stress-free ultra-stable carbon mount is unique. Unlike other designs which operate near the temperatures where chemical instabilities will set in, the ES-423E carbon mount is almost impossible to destroy by accidental over-temperature.

The melting point of lanthanum hexaboride itself is somewhat over 2800 K; there have been examples of crystals being melted (extreme over-temperature), in which the Kimball Physics ES-423E carbon mount survived.

Applications

Electron sources with LaB_6 and CeB_6 cathodes are employed in many brightness-limited electron optical systems like scanning electron microscopes, transmission electron microscopes, electron beam lithography systems, electron accelerators, X-ray sources, free electron lasers and other customer applications.

Lifetimes in excess of 6 months of continuous operation are regularly achieved in commercial SEM's and TEM's with suitable gun vacuum. It is based on a well-proven heater structure. Continuous operation at the full operating temperature improves the thermal stability of the gun and hence beam current stability. Stable beam conditions are achieved immediately, e.g. for performing quantitative EEL or EDX measurements.

Alkali Based Emitters

Whereas Ba based thermionic cathode systems are widely used in vacuum tubes and dominate applications in the lower temperature range from 700–1000°C, there only exist academic investigations on alkali based systems due to their high chemical reactivity with oxygen, water and CO_2. Nevertheless, still lower work functions than for the Ba based systems have been achieved with alkali based systems, so that emission current densities in the range of 2–10 A/cm^2 can be reached in the range 400–600°C. This implies a significant reduction of the heating power.

The first investigations of Cs coated W or Cs on oxidized W substrates were conducted by I. Langmuir and K. Kingdon in the years 1924–1930. For this purpose they used a Cs oven heatable to temperatures of about 100°C coating the substrate with the evaporated Cs. Depending on the equilibrium partial pressure and hence the degree of Cs coverage, emission maxima were observed between 400°C and 700°C [47] (see Fig. 10.18). But such a solution with a Cs oven is impractical for vacuum tubes, is risky and too expensive for commercial applications. The dwell-time of Cs on the surfaces is short and is decreasing with increasing temperature. According to Fomenko [48] the work function of Cs on W (optimum coverage for about a monolayer) is about 1.5 eV, for Cs-O-W the work function F is about 1.44 eV and for Cs-O_2-W ca. 1.2 eV. Lower work functions are obtained on Ni, Ti, ZrC and TaC bases ($F\{\text{Cs-Ni}\} = 1.4\,\text{eV}$; $F\{\text{Cs-Ti}\} = 1.2\,\text{eV}$; $F\{\text{Cs-ZrC}\} = 1.3\,\text{eV}$; $F\{\text{Cs-TaC}\} = 0.85\,\text{eV}$).

For application in thermionic converters A. Makarov et al. [49] investigated Cs films on pyrolytic graphite in an arrangement similar to the one of Langmuir. They obtained a current density of 75 A/cm^2 at 580°C operating temperature and a Cs reservoir temperature of 220°C. They had to cope with the same disadvantages of alkali based systems: a saturation of the tube rest gas with Cs vapour is of course not acceptable.

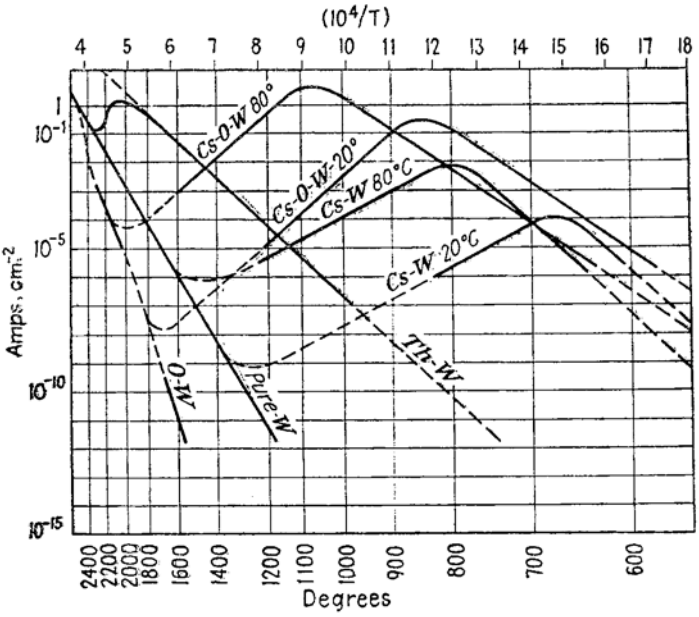

Fig. 10.18. The emission of monoatomic films on tungsten, including Cs on W and Cs-O-W (after Dushman [47])

Only with the introduction of a local supply mechanism of Cs from a moderately heated CsAu compound, the application of Cs based systems with low work function became feasible. This was achieved by Philips in the context of replenishing Cs on semiconductor cold cathodes, which increases the efficiency of ACC cathodes (avalanche cold cathode) by orders of magnitude [50].

Well known is also the application of alkali based photo cathodes with low work functions of 1.5 to 1 eV, where impinging light induces electron emission. Yet this is only possible up to 50°C, since then Cs losses become too excessive. Typical compounds used are K_2CsSb or AgCsO, RbCsSb; in general, multiantimonide-compounds, as given in a review by P. Coates [51]. Low work functions have also been found for conductive Cs suboxides and Cs-Rb binary suboxides, but have not been used so far for any applications.

10.2 Non-Thermionic Electron Sources

10.2.1 Historic Development

Field Emitters

R.W. Wood in 1897 first described field emission as “fireworks” originating from sharp electrode points in his discharge tube. In 1922 J.E. Lilienfeld for the first time

used a pointed cold cathode in an X-ray tube, drawing erratically several mA. He also observed a further activation of the cathode by Cs. In the following years, also with improved vacuum, the field emission (FE) became more stable. It could be shown experimentally that the fields necessary for FE are a factor of hundred lower than predicted by Schottky in 1923 [52]. In 1928 R.H. Fowler and L. Nordheim published their paper with a theoretical description of FE based on electron tunnelling [53]. In 1936 E.W. Müller introduced the field emission microscope using, e.g. a tungsten point source and a phosphor screen [54]. He showed that the emission originated from submicron protrusions on the tip. Later thermo-field emitters were investigated, and recently diamond emitters and carbon nanotubes (CNT) are used for field emission sources in vacuum microelectronic devices and displays.

From Vacuum Microelectronics to Field Emitter Displays

Shoulders proposed 1956 in [55], based on the knowledge how to build manually machined and assembled tubes which could be operated at frequencies as high as 4 GHz [56], that employing the microfabrication technology developed for on-chip large scale integration of micron-sized solid-state devices will allow a revolution to obtain much faster vacuum microelectronic devices having dimensions which are three orders of magnitude smaller. This was thought possible using field emitters as the source of electrons instead of the commonly used thermionic emission from hot filaments. Based on the theory and experiments of field electron emission [57], at Stanford Research International, CA, USA, Shoulders, Brodie and Spindt developed field emission cathodes made from molybdenum [58] and published an extensive review on their development work [59]. Arrays of cathodes with 10 Mio/cm^2 could be produced, which levelled the noise of the single emitter statistically and showed life times in UHV environment exceeding 10 000 hours. These arrays became attractive to develop flat panel displays [60] and cathodes for high frequency vacuum tube devices [61]. More applications are described in a review by Brodie and Spindt [62], see also Table 10.2.

10.2.2 Field Emission Electron Cathodes

Electrons are released from a material surface or from an atom using very different mechanisms. Figure 10.19 gives schematic the mechanism for various electron emission sources. The Brightness, which is the current per unit area emitted into a steradian, is also given. Field emitters represent the class with the highest brightness of all electron sources.

Field emission appears, if at an metallic surface an electric field (E) of the strength of 10^9 V/m is applied. Such field strengths are generated by low voltages at existing sharp edges and very fine tips $E = U/d \sim U/5r$ with d the electrode distance and r the tip radius. A common form of field emitter is an electrolytically etched tungsten wire of 150 µm diameter, which renders a fine tip of 100 nm radius. To obtain this, the wire must be dipped a defined length of, e.g. 2 mm into the NaOH base. When monitoring the resistance of the etch cell, a sharp rise of the resistance

Table 10.2. History: milestones in the development of FED's

1958	Buck and Shoulders (SRI): Proposal of vacuum microelectronic devices using field emitters
1968	Spindt (SRI): Development and production of molybdenum-based field emission cathodes with integrated control grid
1981	Henry Gray (NRL): Lateral Vacuum Triode with Silicon Field Emitters
1985	Robert Meyer: Demonstration of a matrix-addressable monochrome FED
1988	Meyer, Baptist (LETI): develop Mo-emitters on a resistive layer for FED
1993	Pixtech: demonstrates a colour FED; Micron: demonstrates a 1″ colour FED with Si emitters
1993	Kumar (MCC): demonstrates a FED with Carbon Diamond film emitters
1995	Pixtech/Futaba: demonstrate a low voltage FED
1997	Motorola and Candescent-demonstrate a VGA high-voltage colour FED with Mo Spindt-type Emitters
2003	Samsung: demonstrates a 38″ HDTV colour TV with carbon nanotube (CNT) paste emitters

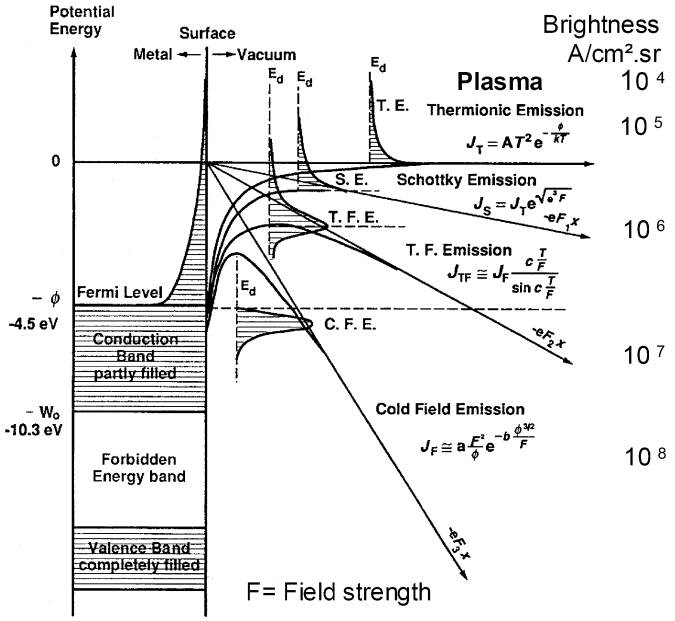

Fig. 10.19. Electron emission mechanisms and brightness of electron sources at 10 kV

will be observed, when the immersed piece of the wire is dropped off due to gravity, and the tip is formed. At this moment it is necessary to cut the voltage off, otherwise enhanced etching will make the sharp tip round. Radii observed are 100 nm with electronic switch-off.

The current density emitted from such tips and edges can reach very high values (e.g. 10^8 A/cm^2). However, the emission currents are generally small (μA, due to the

fact that metals segregate at current densities >250 kA/cm^2 (aluminium)). (Segregation is the disruption of conductors due to ion and atom migration in fields.) In addition, at such current densities an extreme heating of the emitter tip appears and vaporizes this.

10.2.3 Thermo-field Emission Electron Cathodes

To release electrons from a metal surface, the extracting field E_x must be sufficiently strong that electrons can tunnel with a high probability through the potential wall in front of the tip. This wall is the thinnest one close to the tip. At a temperature of 0 K electrons fill the bands in the metal up to the Fermi energy E_F. To have them tunnel from there, a very high field strength of >0.4 V/nm is required. Electrons can however reach energy levels above the Fermi level, by operating the field emitter at elevated temperatures.

Thermionically emitted electrons are not monochromatic, but have a energy distribution with a full width at half-maximum of

$$\Delta E[\mathrm{eV}] = 2.45T[\mathrm{K}]/11\,600. \tag{10.15}$$

Field emission at elevated temperatures is called thermo-field (T-F) emission or Schottky emission. The current obtainable is given by [63]

$$J_{\mathrm{es}} = J_s(\pi q)/(\sin(\pi q)), \tag{10.16}$$

where

$$q = h^{1/4}F^{3/4}/\pi(2m)^{1/2}kT = \hbar e^{1/4}F^{3/4}/\pi(2m)^{1/2}kT \tag{10.17}$$

and

$$J_{\mathrm{s}} = 120T^2\exp\left\{\left(-\Phi + (e^3F)^{1/2}\right)/kT\right\}[\mathrm{A/cm^2}], \tag{10.18}$$

with T the absolute temperature in Kelvin, Φ the work function and F the electric field.

Figure 10.20 shows the potential distribution and the electron distribution in metal at elevated temperature. Since electrons at $T = 0$ fill the metal potential well up to the Fermi level, a high field is required to release them by tunnelling through the potential into the vacuum. Since in a heated metal the electrons above the Fermi level have a Maxwellian energy distribution, they can tunnel at lower field strength and deliver an emission current in thermo-field emission [64].

To increase the emission current, not only heating of a metal tip is used, like with a W <100> thermal field build up tip, but also adsorbed layers are supplied to lower the work function of the material. It has been shown that zirconium, having a work function of 3.9 eV, adsorbs on W <100> planes selectively, by an intermediate layer of oxygen adsorbed to the W-tip. This is schematically shown in Fig. 10.21.

This adsorbed double layer also lowers the work function from 4.6 eV for W down to 2.7 eV for Zr-O-W tip coatings. This reduces the required field strength and extraction voltage, and confines the emission site to the area of low work-function,

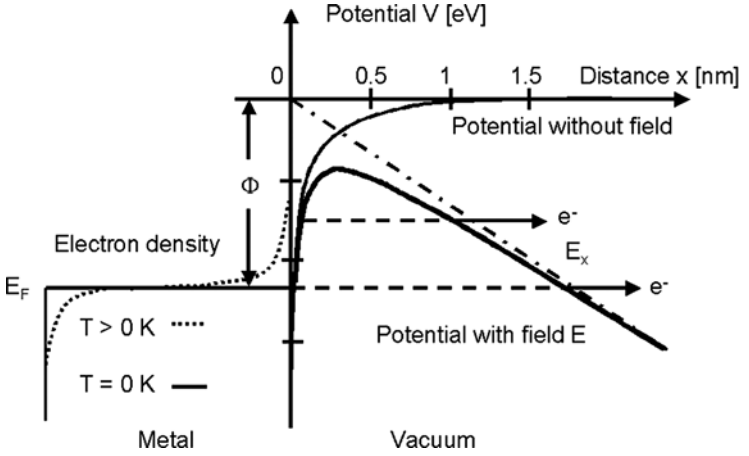

Fig. 10.20. Potential distribution and the electron distribution in metal at elevated temperature, and potentials for tunnelling of electron in T-F emission

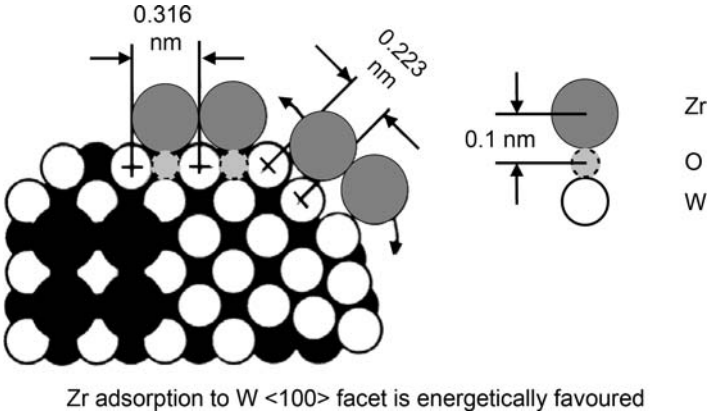

Fig. 10.21. Schematic representation how zirconium adsorbs on W <100> planes of the W-tip selectively by an intermediate layer of oxygen

see Fig. 10.22 [65]. The reduction of emission sites at the cathode renders in a reduced emission current and gives a better beam stability. In addition, it reduces the energy broadening of the emitted electrons due to Coulomb interaction effects.

10.2.4 Cold Field Electron Emission Cathodes

For applications in microscopy and materials analysis the brightest possible cathodes are required. Those are found with cold field emission cathodes. Very fine etched metal tips emit up to 10^8 A/cm^2 current in narrow emission angles. The field emission current density (J_{F0}) at room temperature (300 K) is given by

$$J_{F0} = C_1 E^2 \exp(-C_2/E), \tag{10.19}$$

Fig. 10.22. Field emission microscope observation of emission confinement by absorption of Zr on O on a W field emitter tip

where E is the electric field strength and C_1, C_2 are material constants depending on the work function. At higher temperatures (<1500 K) the emission current density is given by the analytic expression

$$J_{\mathrm{FT}} = J_{\mathrm{F0}}(T R/\sin \pi R) \tag{10.20}$$

with $R = 9.3 \times 10^5 \Phi^{1/2} T/E$, Φ the work function (eV) and T the temperature [K].

The Fowler–Nordheim equation describes the current density obtainable in field emission, taking the image force and geometry into account (see Fig. 10.23 top), by

$$J = (AE^2)/(\Phi t^2(y)) \exp((B\Phi^{3/2} v(y))/E). \tag{10.21}$$

Here, Φ is the work function, E is the field strength, A, and B are factors, $y(\Phi, E)$ is a function of field strength and work function, $y(\Phi, E) = 3.79 \times 10^{-4} \Phi^{1/2}/F$, with $v(y) \approx 0.95 - y^2$, and $t^2 \approx 1.1$ representing the influence of the image force.

For better evaluation of the emission characteristics a logarithmic display of the current density divided by the square of extraction voltage over the reciprocal value of the extraction voltage, generally called the Fowler–Nordheim plot is used (see Fig. 10.23 bottom)

$$\log_{10}(J/U^2) \sim 1/U. \tag{10.22}$$

The extrapolated ordinate value of the FN line is a measure for the obtained reduced current density. The inclination of the FN line corresponds to the work function and the field in front of the emission site.

This field strength is difficult to measure and to determine. Therefore, these data only give relative values. The field strength at the tip depends also on the materials structure, or structure composition, and on the semiconductor characteristics of the material. Fowler–Nordheim equation and logarithmic representation are used to characterize field emission sources. Characteristic data are taken from the inclination and the ordinate section value and are used in SG-plots, showing these data in a graph for different sources.

The major types of field emission cathodes and emitter cells for arrayed field emission cathodes FEA-cells like point emitter (Spindt-emitters (Mo) or Gray-emitters (Si)), wedge emitter, and thin film edge emitter are used. Figure 10.24 shows Spindt-type Mo-emitters.

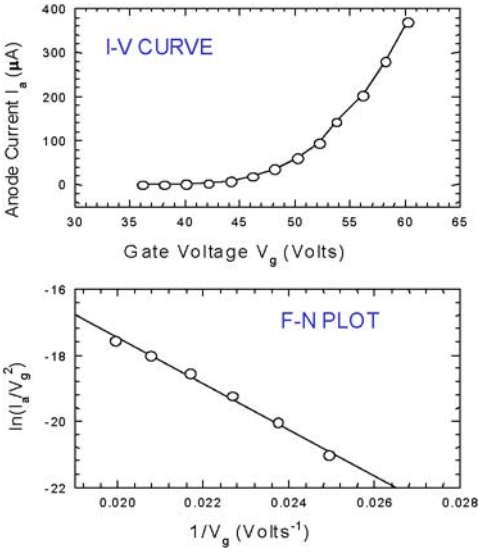

Fig. 10.23. *Top*: current–voltage curve shows the exponential emission characteristic; *bottom*: the logarithmic representation according to Fowler–Nordheim gives the straight line, which allows to judge on the performance

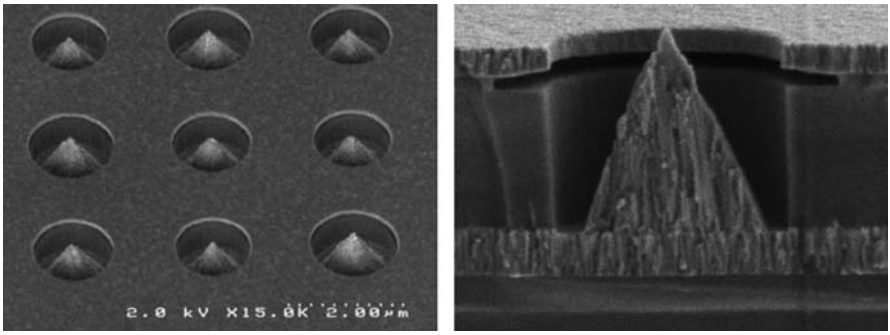

Fig. 10.24. Mo-microtip array of Spindt type (courtesy of C. Spindt SRI). The emission strongly depends on tip height, radius of curvature, position in the gate opening

10.2.5 Novel Cathode Materials

Several novel materials are developed and applied in technical electron sources and FED's, and are given in Sect. 10.2.5, Table 10.3. Novel cathode materials are molybdenum, silicon, diamond, carbon in corraline carbon, carbon nanotubes and semiconductor particles suspended in an oxide matrix (not shown). Also novel materials produced by electron beam induced deposition (EBID) with a nanocrystalline composition are used, e.g. Au/C and Pt/C nanocomposits, see Table 10.3.

Table 10.3. Table of typical performance data of field emission cathodes

Electron sources	Year of market entry	Brightness A/cm^2 sr V	Efficiency	Maximum current
Gas discharge	1930	1	0.05	100 μA
Thermal emitter W	1932	10	0.35	200 μA–15 mA
BaO	1940	100	0.35	50 μA
LaB_6	1960			
Thermofield Zr-O-W	1970	1000	0.40	100 nA
Cold FE	1964	10 000	0.95	5 μA
Spindt-Mo	1970			500 μA
Gray-Si	1985			50 μA
Diamond	1995			200 μA
Carbon nanotubes	2003	10 000	0.95	50 μA
EBID Au/C Pt/C	1992	10 000	0.95	1 mA

10.2.6 Trends of Novel Developments

Field emitter arrays (FEAs) are one of the most important electron sources for vacuum microelectronics. One of the issues arising from FEA processing is incomplete homogeneity in tip shape over the array. Such inhomogeneity gives rise to different emission behaviour among FEAs. Tip surface modifications have been performed for the purpose of obtaining a sharp tip and a clean surface using ion milling [66], reactive ion etching [67] and plasma etching [68], see Fig 10.24. The modification of Si tip surfaces by anodization [69] has been used to improve the emission behaviour of Si FEAs, see Fig 10.25. Tip shape modification using a focused ion beam (FIB) has been performed in order to obtain a sharp tip [70].

Electron-beam-induced deposition (EBID) is caused by the dissociation of adsorbed molecules induced by highly energetic electrons [71]. The dissociation process has not been clarified yet due to the variety of potential excitation channels available even for small molecules. The EBID process facilitates a maskless process down to 5 nm depending on electron beam spot size and reactions. EBID can yield three-dimensional structures on any kind of surface as long as the precursor molecules adsorb [72]. A field emission tip achieved by EBID has been reported, though the structure was that of the two-tip arrangement [73], see Fig. 10.26. Pt-FEA tips with a gate electrode were fabricated by EBID emitter generation in Spindt-type cells having a blunt emitter tip, which showed no emission. The emission characteristics were measured before and after Pt deposition. Nanometer-sized field emitters have also been fabricated using FIB-etching and EBID [74].

Smart FEA structures incorporate a current stabilizing MOSFET transistor and are fabricated in MOSFET Technology, see Fig. 10.27. Transistor-controlled cells with single, dual and triple gate have been developed and employed to stabilize the emission. This leads to a stable intensity [75]. Characteristics obtained were: at gate diameters of 3 μm the onset voltage was 75 V, the maximum current was 10 μA at

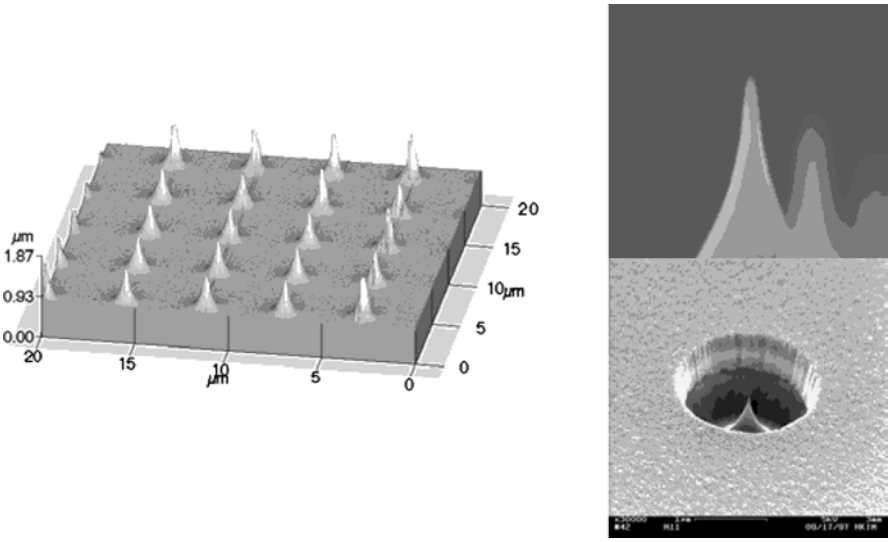

Fig. 10.25. Silicon field emitter arrays (courtesy of T. Akinwande, MIT (1997))

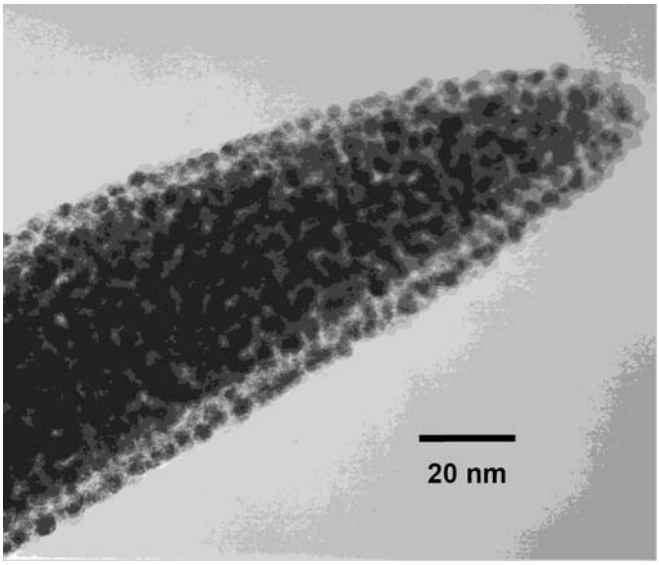

Fig. 10.26. Top of a tip deposited from dimethyl-gold-trifluoro-acetylacetonate (Me2-Au-tfac) at 300 pA and 25 kV shows nanocrystalline composition imaged in a 200 kV TEM

100 V gate voltage and the current stability over 24 hours in a vacuum of 10^{-8} Pa was 25% in a 10 × 10 tip array.

Candescent emitters produced with ion beam technology uses 10^8 to 10^9 ions/cm^2 (random pattern) multiply ionized Xe or Ar at 2 to 13 MeV energy, see Fig. 10.28.

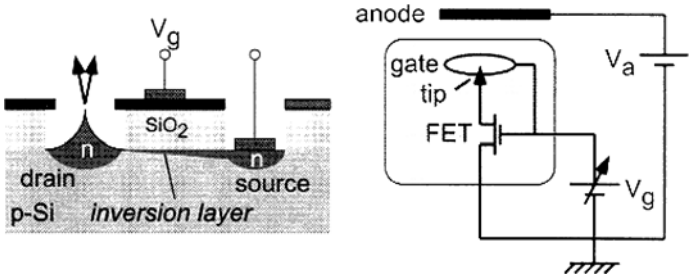

Fig. 10.27. Smart FEA structures incorporate a current stabilizing MOSFET transistor and are fabricated in MOSFET Technology

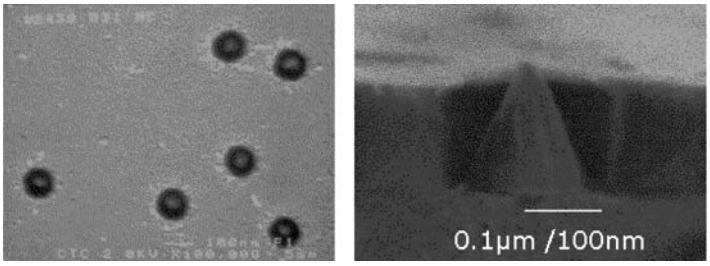

Fig. 10.28. Candescent FED emitters are produced by ion beam irradiation to avoid patterning of extractor holes by electron beam lithography or other methods, like optical holography or ball lens exposure. *Left*: 100 nm scale gate holes. *Right*: 150 nm size emitter cones

A 1 cm^2 diameter beam is rastered over the active area of the display, with a uniformity of <5%. 320 × 340 mm panels are irradiated at the Lawrence Livermore National Lab (LLNL); 60 seconds are needed to iradiate the panel. The successful technology was stopped by financial considerations within the US-Asia powerplay.

10.2.7 Metal–Insulator–Metal (MIM) Emitter Materials

PFE's screen printable cold cathode contains conducting or semi-conducting particles of ≈3 µm in size suspended in an inorganic insulating matrix, generating a metal–insulator–metal–insulator–vacuum (MIMIV) device, which emits electrons by tunnelling, see Fig. 10.29.

Screen printed emitters are used in a 32 × 32 device, as shown below, and have higher particle and emission site density (300 k sites per cm^2), flatter surface, are easier to fabricate, and render ≈30% higher emission uniformity. They require 50 volts swing drive electronics. To make FED's economically competitive, it is inevitable to lower the gate switching voltage to 25 V or below.

10.2.8 Diamond Hopping Electron Emitters

Diamond-like layers have insulating diamond grains in sp3 carbon configuration and grain boundaries in sp2 carbon configuration. The latter are conducting and deliver

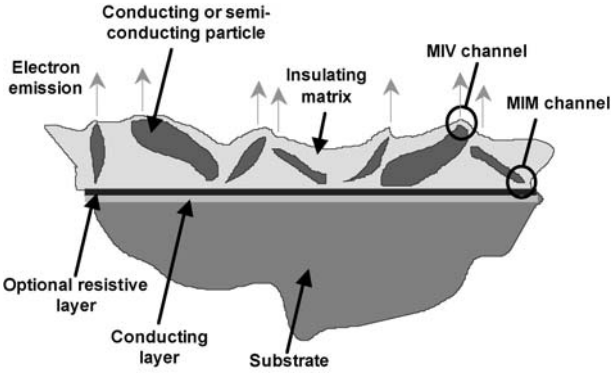

Fig. 10.29. Printable inks made from semiconductor material embedded in insulator matrix present metal insulator vacuum channels for field electron emission after firing (courtesy of PFE Inc.)

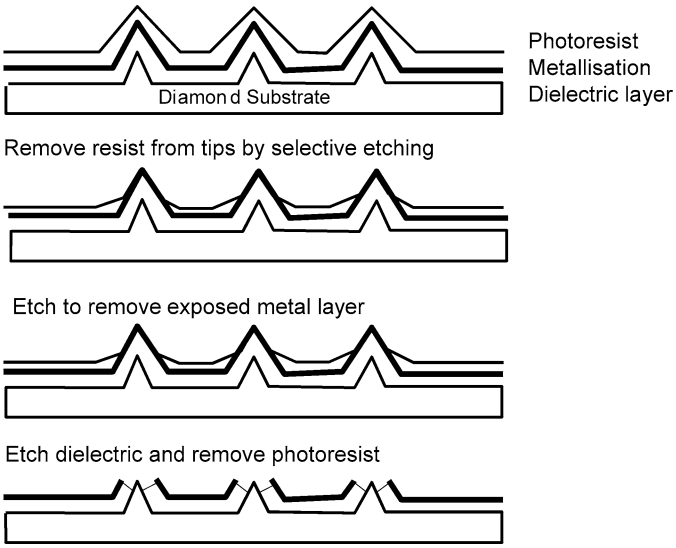

Fig. 10.30. Schematic of the fabrication method for gated diamond emitters

current by hopping. Typically 5–20 V/μm field strength is applied to a diode configuration to characterize such emitters.

Extreme Devices did fabricate CVD gated diamond microtip arrays for high power, high temperature and high radiation environments, see Fig. 10.30. These diamond cathodes shall replace thermionic cathodes in: microwave amplifiers, space applications, sensors, TV-tubes. The gate is self-aligned. Electron-extraction field: 3 V/μm, high-current-density emission: 10 A/cm^2, low onset voltage 22 V. Stable emission over long time, also in high vacuum (courtesy of Extreme Devices Inc.)

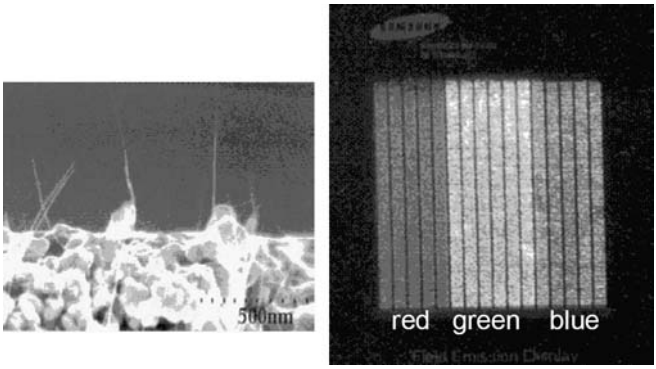

Fig. 10.31. Display with carbon nanotubes from Samsung (courtesy of Choi et al., SAIT Samsung, Korea)

However, flat diamond layers render measured maximum emission current densities for N doped, P doped and B doped diamond all below 4×10^{-5} A/cm^2 [76]. Increased emission is obtained with B doped diamond tips with increased sp^2 content. Emission increases from 1 μA to 20 μA per tip. The turn-on field is 9 V/μm [77].

10.2.9 Carbon Nanotube Emitters

Carbon nanotubes (CNT) grow in gas discharges from butene and other low molecular weight carbon gases and form fullerene-type hoses, which are single to multi-walled and conduct current. Seeding a surface with Fe or Co through lithographicaly generated holes and lift-off allows to select the location of growth of single CNT's. It is possible to fabricate distributed arrays with 5–10 nanotubes/μm^2. They render a bright FED display at 0.2 mm cathode–anode distance and 600 V anode voltage. The maximum current density is 0.1 A/cm^2 [78], see Fig. 10.31.

A much cheaper method to distribute the CNT's than lithography is ink jet printing or sieve printing using CNT filled polymers and optical lithography. Figure 10.32 shows electron emitter sites generated by such a technique. HDTV images with 5″ full colour and moving picture (320 × 240× R, G, B) is shown in Fig. 10.33. Specifications of the Samsung 38″ CNT FED are: screen size 38″ diagonal, pixel number 1280 × RGB × 768, brightness 180–360 Cd/m^2 (F.W.), dark contrast 530:1, power consumption 90 W. Samsung 38″ CNT FED was presented at IVMC 2003 [79], see Fig. 10.33.

10.2.10 Other Carbon Emitters and Future Development Trends

The gate voltage amplifier electronics makes PDP displays expensive. With CVD carbon nanotube gated cathodes the gate voltage is reduced. Emission current density: up to 8 mA/cm^2, Life time at >50% current >10 000 h, cathode material with binder-CNT paste with photolithography structured. This fabrication method allows

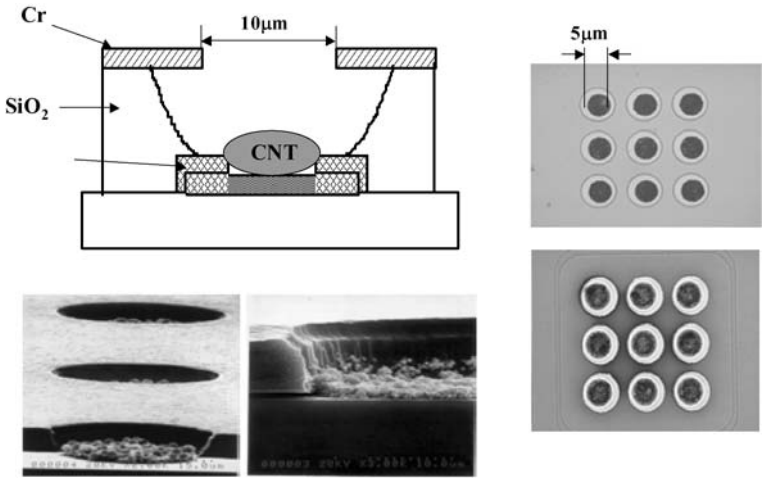

Fig. 10.32. Samsung carbon nanotube FED with a normal thin film gate triode structure. This is possible due to the application of a photosensitive CNT containing cathode paste applied with screen printing methods and UV curing for the definition of the cathode (courtesy of J.M. Kim, SAIT Samsung)

Fig. 10.33. HDTV images with 5″ full colour and moving picture (320 × 240× R, G, B) (courtesy J.M. Kim, SAIT Samsung)

to produce 40″ displays at low cost development at Motorola; gate–anode distance 0.7 mm, anode voltage 3.8 kV, packaged successfully. The onset voltage was 25 V. A major challenge to the display industry is to find low-cost carbon nanotube FED emitters using inexpensive driver electronics [80]. Future possible commercialization will take place in the fields of small displays as replacements of LDC small screens and VGA computer displays. The big FED 30″–50″ display for home TV is a possible major driver for the development. Lamps as picture tube elements, and

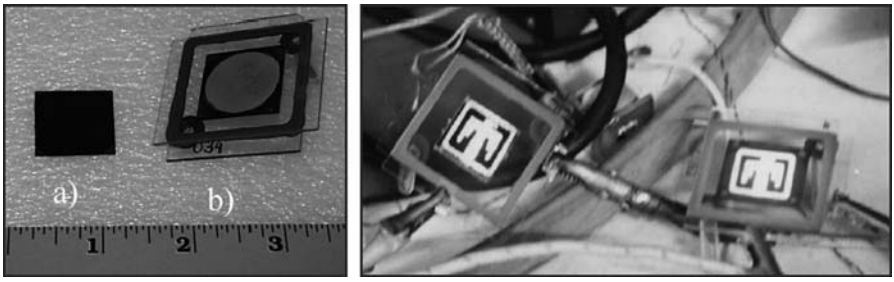

Fig. 10.34. Flat diode lamps, *left*: **a** $1'' \times 1''$ nanotube cathode on silicon substrate, **b** flat panel diode package. Cathode–anode gap is 0.2 mm. Right: blue and red pictured light sources under test. Anode voltage 390 V, brightness 400 cd/m^2 (courtesy of C. Hunt, UC Davis, CA) [81]

also lamps for room lighting are developed and will be mass-produced in the near future.

Flat diode lamps are investigated at UC Davis, CA, in collaboration with Sandia National Laboratories Livermore, CA, and are shown in Fig. 10.34. Table 10.4 gives a comparision of FED with other flat panel displays.

10.3 Other Electron Emitters

10.3.1 pn-emitters

Avalanche Cold Cathodes

Apart from improved thermionic cathodes also low drive cold cathodes are developed. The principle of operation is the avalanche cold cathode [83, 84]. The cold emitter based on silicon IC technology consists of a shallow p^+n^{++}-junction, where the n^{++}-layer has a thickness of 10–20 nm (Fig. 10.35). The internal field of the pn-junction heats the electrons to a much larger temperature than the lattice temperature, and with a Cs covered surface several percent of the diode current are emitted into vacuum at current densities up to 8000 A/cm^2 over an area of about 1 µm lateral extension. One of ACCs main advantages over thermionic cathodes in CRTs is that only a few volts of video-drive are necessary, which leads to a power reduction of the set. Also, excellent picture quality has been demonstrated. Yet sustaining continuous Cs coverage on the ACC surface has led to new vacuum-technological concepts like the addition of a Cs-Au compound thin film for Cs resupply.

As a cathode with low operation voltage for the vacuum microelectronic devices, a new silicon tip avalanche cathode (STAC); which is a silicon field emitter with a shallow n1–p1 junction formed on the tip, is studied [85]. The measured emission characteristics of STAC show that the gate voltage at which an appreciable emission current begins to flow is lowered, and the gate voltage required to produce a desired emission current is reduced. These emission characteristics of STAC result from the hot electrons generated and accelerated by the avalanche breakdown at the n1–p1 junction on the tip, see Fig. 10.36, and Fig. 10.37.

Table 10.4. Comparison of FED with other flat panel displays [82]

Feature	Thin film transistor LCD	Electro-luminescent display	FED	Plasma display panels	OLED display
Brightness (cd/m^2)	200	100	150 (low-V) >600 (high-V)	300	300
Viewing angle (degrees)	±40	±80	±80	±80	±80
Emission efficacy (lm/W)	3–4	0.5–2	1.5–3 (low-V) 10–15 (high-V)	1.0	10–15
Response time (ms)	30–60	<1	0.01–0.03	1–10	<0.001
Contrast ratio (intrinsic)	>100:1	50:1	300:1	100:1	100:1
Number of colors (Mio)	16	16	16	16	16
Number of pixels	1024 × 768	640 × 480	800 × 600	852 × 480	640 × 480
Resolution mm in pitch	0.31	0.31	0.27	1.08	0.012
Power consumption (W),	3	6	2	200	6
Size (cm)	25.4	25.4	25.4	106.7	15.2
Maximum screen size in diagonal (cm)	55.9 (22″)	25.4 (10″)	35.6 (14″)	106.7 (42″)	15.2 (6″)
Panel thickness	8	10	10	75–100	3
Operating temperature range (°C)	0–50	−5–±85	−5–+85	−20–±55	−25–±65

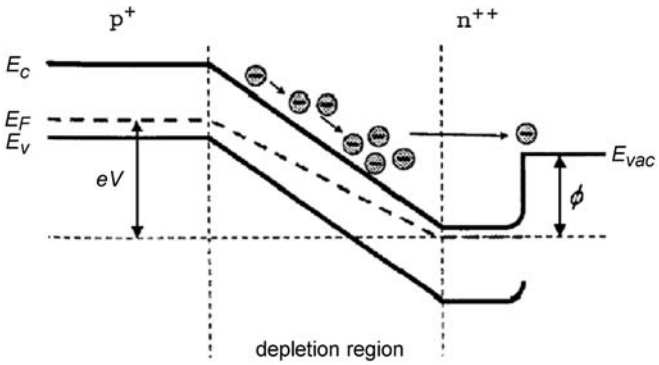

Fig. 10.35. Electron energy band diagram of an avalanche cold cathode driven in reverse bias. Electrons generated in the depletion layer are accelerated towards the surface

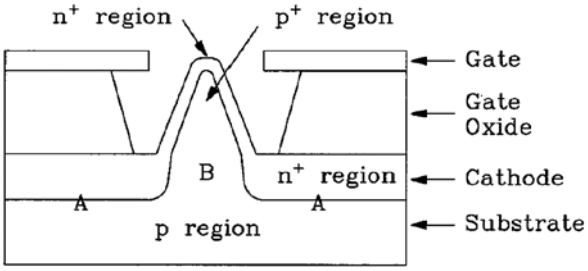

Fig. 10.36. Practical design of an ACC-field emission source (after Lee [85]), a shallow n-p junction is formed at the tip by lithographic steps and ion implantation to $10^{15}/\text{cm}^2$

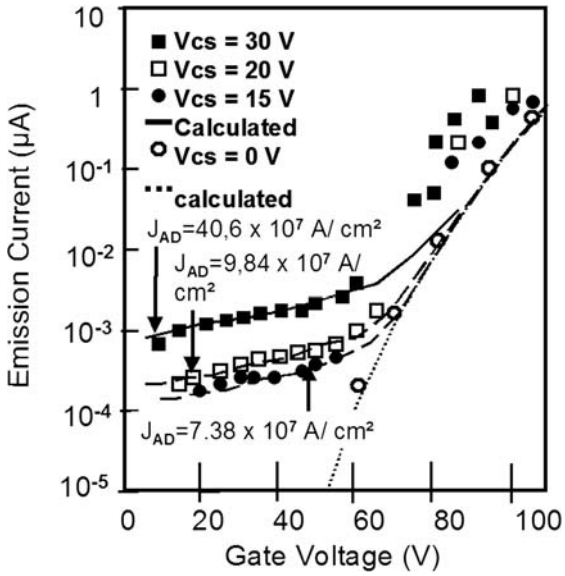

Fig. 10.37. Comparison between the calculated emission current curves (*solid line*) for $J_{\text{AB}} = 7.38$, 9.84, and 40.63×10^7 A/cm^2 and the measured emission current data for $V_{\text{CS}} = 15$, 20, and 30 V. Also, the calculated emission current curve (*dashed line*) and the measured emission current data for $V_{\text{CS}} = 50$ V are shown [86]

The low gate voltage characteristics of STAC is well explained by a simple analysis which takes into consideration the emission of hot electrons. However, the measured emission current of STAC in the high gate voltage region is not well resolved by the analysis. Also a large current is needed for the avalanche breakdown, and this results in low emission efficiency and large power consumption.

Ballistic Electron Emitters

The mechanism of ballistic electron emission from nanocrystalline silicon diodes is obtained from nanocrystallized polysilicon (NPS) based devices. The electron

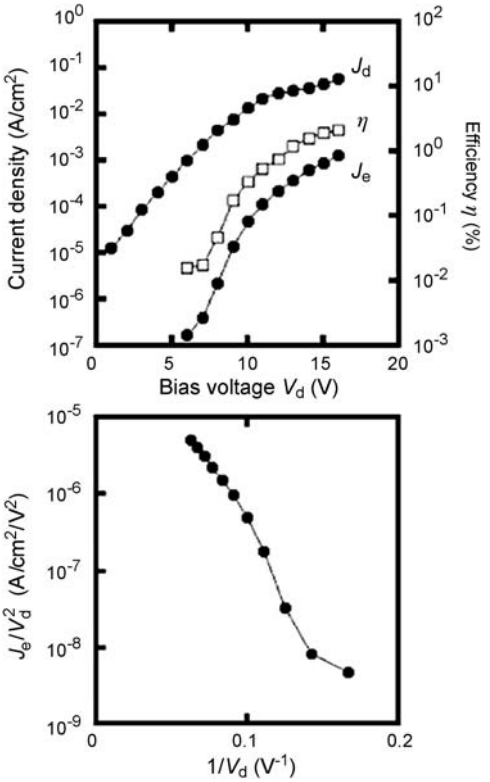

Fig. 10.38. The emission current curve and the diode current curve. Both determine the efficiency h, which is as low as 2.8%

emission characteristics performs due to of chainlike nanocrystalline silicon ~nc-Si structure, which is produced along columnar poly-Si grains. A sufficient electron emission current density of 3.0 mA/cm^2 was observed with a high emission efficiency ≈2.8% and stability, see Fig. 10.38. The surface and interfacial oxidation of nc-Si particles is an important factor for efficient emission. The results indicate that control of interconnected nc-Si structures is a key issue for the efficient ballistic electron emission [86]. It is found that nc-Si chains interconnected via thin oxides play a key role for efficient electron emission. This supports the ballistic electron transport model based on multiple tunneling in the nc-Si layer [87, 88].

10.3.2 Secondary Emission

For a detailed description see Sect. 3.2.2.

10.3.3 Ferroelectric Electron Emission

Weak electron emission during polarization reversal of ferroelectric material was first reported by Rosenman et al. in 1984 [89]. The spontaneous electrical polarization of ferroelectric materials can be changed either by reversal or phase transition between ferroelectric and non-ferroelectric state. If spontaneous polarization changes are induced by fast temperature rise, by a mechanical pressure pulse, by a laser pulse or a high voltage pulse applied to the sample, strong uncompensated surface charge densities and related polarization fields are generated, which may lead to intense self-emission of electrons from negatively charged surface areas. Thus, in electron guns the extraction-field free emission can be separated from high field regions of accelerating gap or gate structures. In 1988 at CERN strong ferroelectric pulsed electron emission of up to 100 A/cm^2 was achieved. Inherently dc-emission is not possible with this principle. The first application was the use of ferroelectric emission as a trigger to ignite the discharges of high power gas switches. Another application was the alternating gradient space charge focussing of low energy heavy-ion beams, i.e. for an accelerator technology.

10.3.4 Photo-electron Emission

Photoelectric emission is the emission of electrons caused by the irradiation of matter by light. Fundamentals are described in Sect. 3.2.1. It is investigated in dependence of the existence and properties of solid surfaces. Photoemission occurs in the fundamental optical range. Thus, it is related to other optical experiments and is used for solid state spectroscopy, i.e. the determination of band structure. In theories of electron emission one generally assumes that all electrons whose energy associated with the movement normal to the surface is larger than the potential in vacuo can escape. Thus, the probability of escape P is taken to be

$$P = 1 \quad \text{if } E - n^2 k||/2m > U_{\text{vac}}, \tag{10.23a}$$

$$P = 0 \quad \text{otherwise}, \tag{10.23b}$$

where $k||$ is the wave vector parallel to the surface, m is the free electron mass, and U_{vac} is the asymptotic value of the potential in vacuo. In reality, electrons satisfying (10.23a) are partially reflected because of diffraction by the periodic potential of the solid. It is not generally possible to match a Bloch wave in the solid with a single plane wave in vacuo without the existence of reflected Bloch waves. Considerable reflection occurs at low electron energies and therefore $P(E)$ exhibits a pronounced structure. Since diffraction is highly directional, its effect on energy distributions of photoelectrons will be larger in measurements accepting electrons in a small solid angle of directions. In hemispherical retarding field analysers diffraction effects will be approximately averaged out.

The energy diagram of the surface of a semiconductor shows Fig. 10.39. It is characterized by a space charge near the surface that is compensated by a surface charge, S, composed of electrons occupying surface states. These charges produce a

macroscopic potential $V(x)$. Electrons are retained in the material by the potential $U(x)$ which has the shape of the image force at large distances in vacuo. It is characterized by the work function Φ, the electron affinity χ and the ionization energy ξ, as shown in Fig. 10.39. All these quantities can be measured by photoemission. The relationship between $\mathrm{d}V/\mathrm{d}x$ at $x = 0$ and $(E_\mathrm{F}–E_\mathrm{V})_\mathrm{s}$ is particularly interesting, because it yields information on surface states. The surface of a metal is much simpler. It is fully defined by the work function $\Phi = U_\mathrm{vac}–E_\mathrm{F}$.

Band bending near the surface of semiconductors is attributed to charge carriers residing in surface states. In principle, these electrons can be excited by the incoming light and contribute to photoemission. Their observation is facilitated in n-type semiconductors by the fact that electrons in surface states have higher energies than valence electrons. They are isolated at the high-energy end of energy distributions. Experiments with cesiated InAs have shown that, indeed, emission from a few as 0.01 electrons per surface atom could be observed [90]. The Schottky effect in photo emission is the reduction in work function and resulting increase in emission caused by the application of an electric field normal to the surface. This increase in current is a monotonic function of the applied field.

The vectorial photoeffect intrigued early investigators of photo emission and has been relatively neglected in the more recent years. When linearly polarized light falls on a surface at an oblique angle and the components of the electric field parallel and normal to the surface transmitted into the solid are calculated according to Fresnel's equations, it is found that the component of the electric field normal to the surface is much more efficient in producing photoemission than the tangential component. In thin films of simple metals, the enhanced photoemission for E_s is accompanied by an equal enhancement of optical absorption. Both can be accounted for by excitation

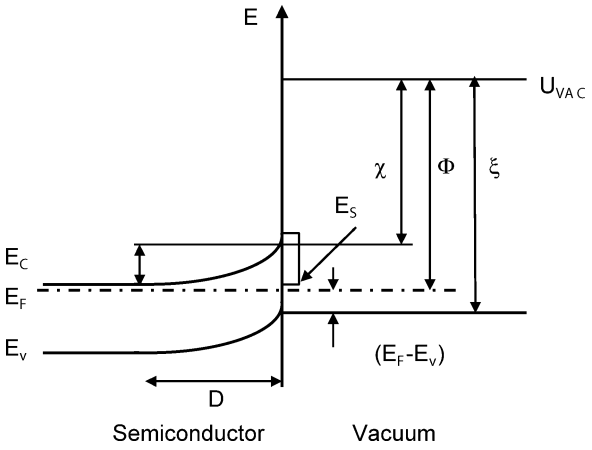

Fig. 10.39. Energy diagram of a semiconductor surface; V_B is the band bending, E_F is the Fermi level, E_c and E_v are the edges of conduction and valence band, E_s is surface states, χ is the electron affinity, Φ is the work function, ξ is the ionization potential and U_Vac is the asymptotic value of image force potential

Table 10.5. Characteristics of standard photocathodes in use

Photo cathode	Sensitivity efficiency μA/lm	Dark current density A/cm^2	Quantum detection efficiency	Wavelength nm
Ag-O-Cs	30 (75)	$10^{-13}..10^{-11}$	1	1200
Alkaline-antimony	50–250	$10^{-18}..10^{-14}$		600–870
Multi-alc-antimony	250–600	10^{-15}	20–25	950
NEA	500–2000	10^{-15}	10–50	1200

of plasma oscillations by the light. The vectorial photoeffect decreases drastically as the film thickness increases beyond 100 nm.

Angular distribution of emitted electrons yields considerable information on the band structure of crystals from which the electrons were emitted without appreciable scattering. It was shown for clean silicon and germanium surfaces, that electrons are preferentially emitted in directions that depend on the crystallographic orientation of the plane of polarization of normally incident, linearly polarized light. This effect shows the presence of a substantial fraction of electrons that were excited by direct transitions and emitted without scattering. These measurements do not rule out the presence of some scattered electrons.

It was observed from the investigation of the angular distribution of electrons emitted from a GaAs crystal, whose surface was covered with Cs and CsO to produce a negative electron affinity, that the electrons were emitted preferentially in a very narrow cone normal to the surface. The angular distribution was found to be Gaussian, with a half-width that depends on wavelength of UV-light and surface treatment but is of the order of 10 degrees. The explanation of this effect is that the majority of the electrons that have been excited at great depth ($\approx$1 μm) have lost their kinetic energy and are "thermalized" in the bottom of the conduction band ($k = 0$). They are accelerated in a direction normal to the surface by the space charge field and emitted after negligible scattering at the surface. For more details and literature, see Fischer 1972 [91]. Table 10.5 summarizes the characteristics of standard photo cathodes in common use.

Inclusion of getter materials in a cavity allows to operate handheld vacuum photosensitive electronic devices on a chip. Getter materials are used to disperse alkali coatings of surfaces for photo-sensible structures. Alkali metal dispensers (AMDs) are compact sources of alkali metals. They may be used to prepare photosensitive surfaces of photo cathodes or wherever an ultrapure alkali metal film is needed. The alkali metal generating source is a mixture of an alkali metal chromate with a reducing agent. A research program at SAES Getters S.p.A. into methods of controlling the release of pure alkali metals led to the development of SAES AMDs. SAES alkali metal dispensers are especially suitable when very pure alkali metal films are required, evaporation rate must be controllable and reproducible and loose particles cannot be tolerated. The device must be free of harmful gases during deposition of

the alkali metal. The reducing agent in SAES AMDs is SAES' St101 (Zr 84%-Al 16%) getter alloy. In addition to reducing the alkali back to its metallic state, St101 also removes chemically reactive gases from the device preventing them from contaminating the alkali metal vapor. SAES AMDs are available to deposit Cs, K, Na, Rb and Li. They are available in precut sizes with terminals or in bulk wire. Curved shapes are available [92].

10.4 Vacuum Electronic Construction

10.4.1 Spacers for FEA's

To separate the cathode plate and the screen plate in a FE-display, spacers are required. It is not sufficient to have insulators, but semiconductors or resistive supports are required to assure the proper function of the display. Researchers from Saint-Gobain Display Glass, France, could solve the problem by making a semi-conducting glass. Figure 10.40 shows a cross-spacer which fits in between pixels and does not attenuate the electron beam at his site. Several spacers are to be distributed over the area of a large display at least in 1 to 5 cm distance depending on the thickness of the glass sheets. Earlier solutions were made from ionic conducting glass [93].

10.4.2 Anodic Bonding

Anodic Bonding

The substrates are bonded at elevated temperature (≈400°C) by placing and clamping the substrates between two metal electrodes. A high DC potential (up to >1 kV) is applied between the electrodes creating an electrical field, which penetrates the substrates. One substrate is a glass that contains sodium ions, which at the elevated temperature are displaced from the bonding surface of the glass by the applied electrical field. The depletion of sodium ions near the surface of the glass makes the

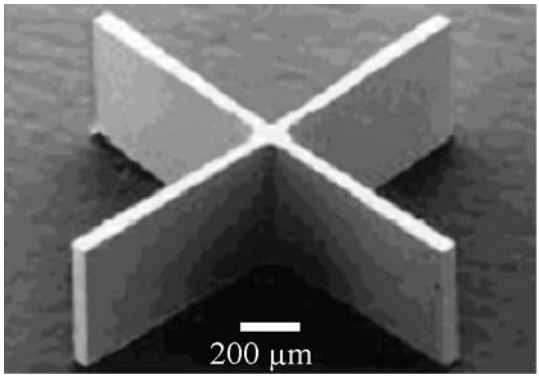

Fig. 10.40. Semiconducting glass cross spacer, which fits in between pixels and does not attenuate the electron beam at his site (curtesy of Saint-Gobain Display Glass, France)

surface highly reactive with the silicon surface of the other substrate forming a solid chemical bond.

Fusion Bonding

The substrates are first forced into intimate contact by applying a high contact force. Once in contact the substrates hold together due to atomic attraction forces (Van der Waals), which are strong enough to allow the bonded substrates to be handled. The substrates are then placed in a furnace and annealed at high temperature, after which a solid bond is formed between the substrates.

Glass Frit Bonding

The alignment tolerance for registration of CAD data to features on the wafer is typically 10 μm. A batch process is possible. The second substrate material may be e.g. Pyrex (Corning 7740) having a substrate diameter of 50 mm and a substrate thickness of 300 to 1000 μm. Bonding takes place at a temperature of 400°C. Silicon wafers may have up to 100 mm wafer size.

Solder Bonding

A gold metal layer is employed on both sides of the parts to be bonded. The alignment tolerance is 5 μm to 200 μm if needed. Alignment is performed manual optical. The substrates are exposed to a vacuum of 0.1 mb during processing. The gold is bonded at a temperature of 350 to 450°C.

Epoxy Bonding

Epoxy bonding is performed in air, with alignment. It is necessary to use Piranha (H_2SO_4/H_2O_2)clean (non-MOS clean) on both surfaces. If there are metal parts on any of the wafers, select an organic NMP clean. Epoxy coat the front to a thickness of 5 μm to 8 μm. Three methods for alignment are possible: optical implies front-front align, backside IR implies front-back align, manual implies no fine alignment.

Bonded materials are preferred pairs of materials bonded by this process glass (Hoya), Pyrex (Corning 7740), silicon, silicon on insulator. The pressure in the process chamber during processing is 1 atm. Wafers of 75 to 100 mm in size can be bonded.

Resist Bonding

This process requires several steps: (1) dehydration bake both surfaces, (2) prime front with HMDS, (3) photoresist coat front with resist material Shipley 1827 of 2.7 μm thickness, (4) resist bond both, (5) perform photoresist hardbake (110°C) both parts. This process is applicable to wafers of 25 mm to 100 mm diameter.

Other Bonding Processes

They are: aluminum microwave bonding, copper microwave bonding, gold microwave bonding, nickel microwave bonding, thermocompression bonding, adhesive bonding, eutectic bonding, low-temperature glass bonding, microwave bonding [94].

10.4.3 Vacuum Generation in On-Chip Vacuum Electronic Devices

Inclusion of getter materials in a cavity allows to operate handheld vacuum electronic devices on a chip. Getter materials chemically bond residual gases and generate vacuum for a long time. SAES Getter supplies a St707 getter alloy for vacuum systems. The St707 wide operating temperature range down to room temperature and its availability in different formats make this alloy the best solution for several applications, from particle accelerators to plasma fusion machines, from laboratory vacuum systems to batteries. It is a getter material composed as a ternary alloy with the following nominal composition: zirconium 70%, vanadium 24.6%, iron 54%. To pump the St707 getter needs activation, since it has a protective passivation layer that must be eliminated to start the gettering action. This process, called activation, is carried out by heating the getter under vacuum or in an inert gas atmosphere. The optimum activation conditions are at 450–500°C for 10 minutes. Once the alloy is activated, reactive molecules such as O_2, H_2O, N_2, CO, CO_2 and H_2 are adsorbed via a three step adsorption mechanism: surface dissociation, surface sorption and bulk diffusion. Hydrocarbons are adsorbed at lower pumping speed at temperatures above 200°C. Once adsorbed, oxygen, nitrogen and carbon atoms cannot be released by the St707 due to the formation of strong chemical bonds with the alloy atoms. Hydrogen reacts differently: it diffuses into the St707 getter bulk even more quickly than the other species and it distributes almost uniformly within the bulk even at low temperatures. However, since the bonds hydrogen-alloy are weak, some of the hydrogen sorbed at low temperatures can be released at higher temperature. The sorption speed for various gases at different temperatures for ST707 getter from SAES Getter shows Fig. 10.41 [94].

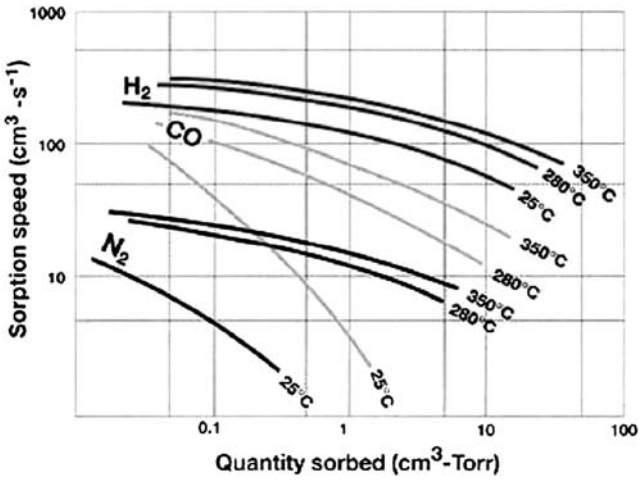

Fig. 10.41. The sorption speed for various gases at different temperatures for ST707 getter from SAES Getter

Nanogetter Packaging

The process is complex and needs the following steps: (1) silicon cap wafer preparation, (2) nanogetter deposition and patterning; the nanogetter deposition is performed using a specially fabricated shadow mask; the nanogetter is deposited by sputter-deposition, (3) fusion bonding with alignment requires a pre-fusion-bond clean of both surfaces to be bonded, a fusion pre-bonding of both surfaces and finally a nitrogen anneal of both parts.

As bonding method can be used anodic bonding (Si to Pyrex), eutectic bonding, fusion bonding (Si to Si direct) or glass-frit bonding. As capping material Kovar Pyrex (Corning 7740) on silicon is recommended. To incorporate the getter or other device, a cavity etch produced by MEMS silicon micromechanical etching is needed [95]. Typically the depth of the etch in the capping wafer is 10 to 550 μm depending on wafer thickness. The thickness of the nanogetter to be deposited must be 5 to 500 nm. A through wafer etch is sometimes performed for electrical connections through the capping substrate.

10.5 Materials of Vacuum Electron Sources

Suitable materials for vacuum technology [96–98] have to meet special requirements with respect to sustaining high pressure differences of up to 15 orders of magnitude between vacuum and outside atmospheric pressure and obtaining constant operating conditions. Dependent on the applications and on the pressure range different groups of materials are used:

1. materials for the vacuum chambers (stainless steel, glass, oxide ceramics);
2. materials for components such as pumps, connecting tubes, valves, flanges and traps (stainless steel, Al, glass);
3. materials for seals (Cu, Au, Fe-Co-Ni alloys, Ag containing solders, Mo, Konstantan, etc.);
4. materials for inner system parts (stainless steel, W, Ta, Mo, Ni, Pt, Ag, Au, Pd, Al, Be, Zr, Ti, diamond, etc.);
5. emitter materials for electron sources (BaO, CaO, SrO, W, Mo, ThO_2, La_2O_3, LaB_6 , Cs, Si, C, etc.).

The choice of a material depends on properties such as high mechanical stability, low gas permeation, low vapour pressure, good heating properties for degassing and good matching of thermal expansion coefficients for different system parts or on special properties such as high electron emission. Further classes of materials are getter materials for pumping and luminescent materials for display screens. A much more detailed description is given in the book of Walter H. Kohl: “Materials and Techniques for Vacuum Devices” [98] and also in the following Chapter 11, “Vacuum Technology”. A large part of the materials given above is also used for vacuum electron source construction, and in the following we will specifically stress this application.

Metals

The following table (Table 10.6) gives a review of metals usually applied in vacuum technological applications. In general, a metal consists of many small crystallites. The form and size of these crystallites determine the mechanical properties. Fine

Table 10.6. Materials for vacuum technology applications

Metal	MP (K)	Density ρ ($g\,cm^{-3}$)	Application examples
Stainless steel	1,803	7.86	Vacuum vessels, flanges, valves, pumps
Fe-Co-Ni and Fe-Ni alloys	1,723	8.2–8.3	Feedthroughs in glass and ceramics (sealing–in process)
W	3,640	19.3	Components for high temperatures, cathodes
Ta	3,270	16.8	Anodes, grids, cathodes
Mo	2,890	10.3	Cathodes, anodes, arc electrodes
Pt	2,046	21.4	Feedthroughs in soft glass, coatings of glass and ceramics
Pd	1,828	12.0	Hydrogen leaks, leakage detectors
Au	1,336	19.3	Vacuum solder, coating for grids and sockets
Ag	1,233	10.5	Solder component, coating of electrical conductors, sockets and copper electrodes
Ni	1,730	8.9	Anodes, grids, shields, oxide cathode bases
Cu	1,356	8.9	Vacuum seals, cooling walls, conductors
Al	932	2.7	Deflection plates, electron windows
Be	1,553	1.85	X-ray windows
Ti	1,963	4.52	Anodes, grids, getter material
Zr	2,403	13.1	Getter material
Ba	987	3.5	Cathodes, getter materials
Cs	301.7	1.9	Cathodes

and elongated crystals (hard-rolled) make the metal hard and brittle. During longer heating above the so-called recrystallization temperature T_R, larger crystallites are formed, whereby the metal becomes softer and ductile (soft anneal). As a rule, the recrystallization temperature T_R can be derived from the melting temperature by

$$T_R = 0.4T_S.$$

Ductility is one of the criteria for good machineability/formability of the respective metal. At heating, at insufficient deformation or at too high temperature very large crystals are formed, and the metal gets brittle. The strength of metals and other materials is usually determined by applying a load to the material under study and by observing the resulting deformation.

Drawn, rolled or pressed metal forms are useable in vacuum technology. Alloys can only be used if the components still have a sufficiently low vapour pressure at the highest operating temperature. Only forming/machining methods are allowed, which do not lead to micro-leaks (e.g. deep drawing, arc erosion, laser cutting). One of the most important materials for UHV chambers and electron guns is wrought stainless steel. Stainless steels are defined as iron–base alloys containing at least 12% of chromium. The type of the stainless steel used (there are more than 37 compositions) will depend on the specific application.

The refractory metals W, Mo, Ta and Nb are of primary interest for electron device construction. Their principal merit is their mechanical strength at elevated temperature which is an approximate function of their (high) melting points. Among these tungsten exhibits the highest transition temperature from ductile to brittle behaviour of 350°C. Hence Mo with a transition temperature of about 0°C is still machineable, whereas W needs powder metallurgical methods for forming, e.g. porous tungsten only becomes machineable when the pores are filled with copper. In general, the choice of metals becomes more and more limited the lower the pressure in the vacuum system is required to be. For UHV chambers only stainless steel, copper and gold are appropriate, but for cathode bases and anodes also W, Mo and Ta are used.

Figure 10.42 shows an example of a UHV diode emission test flange as used by Philips Research. Here the material of the so-called ConFlat flange, the feedthroughs and the mounting posts are made of is stainless steel, the insulating part of the current feedthroughs consists of glass ceramics, whereas the anode is made of Ta and the cathode unit is a combination of a $4BaO{\cdot}CaO{\cdot}Al_2O_3$ impregnated tungsten pill in a Mo cap. The cathode to anode distance is 0.3 mm. The insulation here is obtained by quartz cylinders. This flange is then mounted via a copper gasket on the corresponding flange (inner width 35 mm) of the UHV chamber (made of stainless steel) and is tightend by six screws with controlled rotary torques.

Glass, Glass Ceramics and Ceramics

Although glass is a solid in the sense that it has the rigidity that is generally associated with solid bodies, it lacks the continuous crystalline structure that is characteristic for metals and ceramics. On cooling down of the melt, the liquid state is “frozen

Fig. 10.42. UHV diode emission test flange with a 0.65 W I cathode unit below the Ta anode on top, as used by Philips Research (courtesy of Philips Research Aachen)

in", which means that on cooling down no crystals are formed because the viscosity increases sufficiently fast. At a viscosity of more than 10^{12} Pa s (transformation point) glass transforms from a plastic tension free state to an elastic brittle state. The transformation temperature is essential for glass machining, because this is the lower boundary for decrease in tension in glass in a reasonable time. Glass does not possess a sharply defined melting point where liquid and solid phases exist in equilibrium, but looses its solid-like character gradually on heating. The ease of forming and the ease of sealing to metals are two of the advantages of glass. Further properties of glass important for vacuum technology are a reasonable mechanical strength, but fragility and low shock resistance, chemical and thermal robustness, low vapour pressure, low electrical conductivity, transparency to radiation/good visible light transmission and reasonable cost. The main glass constituents besides SiO_2 are B_2O_3, Al_2O_3, CaO, PbO, K_2O, Na_2O and others.

Glass ceramics consist of a mixture of crystals and a residual glass phase. It is prepared by adding nuclei for crystal growth such as TiO_2 or ZrO_2 to the glass melt, which after cooling down and heating up again grow to larger crystals. Glass ceramics have a higher density, higher viscosity and higher mechanical strength than glass. The thermal expansion can be nearly zero, since the thermal expansions of the crystals and the residual glass phase nearly compensate each other.

Modern ceramics are crystalline sintered materials of pure Al_2O_3 or BeO, which are produced at temperatures far below the melting point. They exhibit high values of thermo-mechanical stability, of chemical robustness and of the specific electrical resistivity and are not permeable for gases also without glass coating. They are used for vacuum chambers of particle accelerators, for corrosion resistant vapour beams and for the insulation of current feed-throughs.

Emitter Materials

The emitter materials used in electron sources again can be divided into metals/elements (see above, including Si, C) and compounds such as oxides, especially of the alkaline earths and of the scandium group, and of the rare earths. Among these we will only address the last three groups of oxides, since they are the most important for low temperature emitters and are not treated elsewhere. Usually, the alkaline earth oxides are prepared in the form of carbonates and then have to be transformed into oxides at elevated temperature, typically under UHV. In nearly all cases the oxides are then used as sources of the respective metals via a suitable chemical reaction in order to form, e.g. a Ba monolayer on the cathode surface either on a metal or an oxide base with a very low work function. Due to the low melting temperature and high vapour pressure of Ba, Ca and Sr this indirect way of Ba, Ca or Sr supply has to be chosen, and hence these cathodes are either oxide or dispenser cathodes. The vapour pressure p of BaO, CaO and SrO are shown in Fig. 10.43 as a function of temperature, the vapour pressure of the respective metals are depicted in Fig. 10.44. Even more critical for UHV is the use of Cs. Here a unique new way is the use of controlled Cs resupply from a CsAu compound.

The oxides of the scandium group and of the rare earths are in most cases only used in small quantities as dopants, e.g. of barium-based oxide cathodes, or as mixed oxides, e.g. Ba-Scandate in the case of Scandate cathodes.

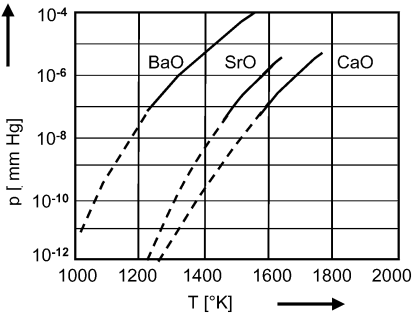

Fig. 10.43. Vapour pressure p (in mmHg = Torr) of alkaline earth oxides as a function of temperature (according to Herrmann and Wagener [97])

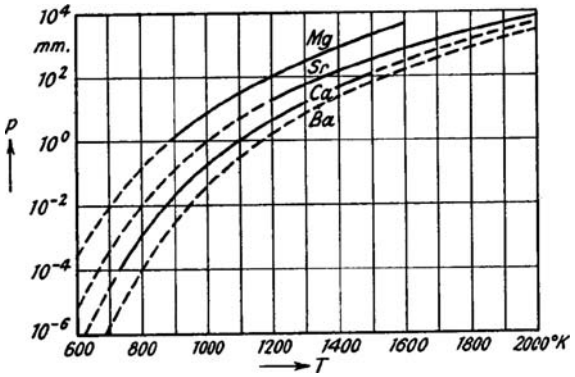

Fig. 10.44. Vapour pressure p (in mmHg = Torr) of alkaline earth metals as a function of temperature [2]

References

[1] F.R. Paturi, *Chronik der Technik* (Chronik-Verlag in der Harenberg Kommunikation, Dortmund, 1989)
[2] G. Herrmann, S. Wagener, *The Oxide Coated Cathode* (Chapman & Hall, London, 1951)
[3] G. Haas, R. Thomas, Thermionic sources for high brightness electron beams, IEEE Trans. Electron Devices **37**(3), 850–861 (1990)
[4] A. Wehnelt, Über den Austritt negativer Ionen aus glühenden Metallen, Annal. Phys. Ser. 4 **14**, 425–468 (1904)
[5] L.S. Nergaard, Electron and ion motion in oxide cathodes, in *Halbleiter-probleme,* Bd. 3 (F. Vieweg-Verlag, Braunschweig, 1956), pp. 154–206
[6] A.L. Reimann, *Thermionic Emission* (Chapman & Hall, London, 1934)
[7] G. Gaertner, P. Geittner, H. Lydtin, A. Ritz, Emission properties of top-layer Scandate cathodes prepared by LAD, Appl. Surf. Sci. **111**, 11–17 (1997)
[8] G. Miram, A. Cattelino, Life test facility for thermionic cathodes, in *TRI Service/NASA Cathode Workshop*, Cleveland, Conf. Record, 1994, pp. 233–236
[9] J. Eichmeier, *Moderne Vakuumelektronik* (Springer, Berlin, 1981)
[10] W. Nottingham, Thermionic emission, in *Handbuch der Physik*, ed. by S. Flügge. Elektronen-Emission/Gasentladungen I, vol. 21 (Springer, Berlin, 1956), pp. 1–175
[11] G. Haas, R. Thomas, Thermionic emission and work function, in *Techniques of Metal Research*, Vol. 6/1, ed. by E. Passaglia. (Interscience Publ., 1972), pp. 94–262
[12] A.G. Knapp, Surface potentials and their measurement by the diode method, Surf. Sci. **34**, 289–316 (1973)
[13] J. Hasker, Calculation of diode characteristics and proposed characterization of cathode emission capability, Appl. Surf. Sci **16**, 220–237 (1983)
[14] C. Herring, M. Nichols, Thermionic emission, Rev. Mod. Phys. **21**(2), 196 (1949)
[15] J. Eichmeier, H. Heynisch (ed.), *Handbuch der Vakuumelektronik* (R. Oldenbourg, München, Wien, 1989)
[16] R.O. Jenkins, A review of thermionic cathodes, Vacuum **19**(8), 353 (1969)
[17] I. Langmuir, The electron emission from thoriated tungsten filaments, Phys. Rev. **22**, 357–398 (1923)
[18] I. Weissman, J. Appl. Phys. **36**(2), 406 (1965)

[19] G. Gaertner, D. van Houwelingen, Electron emission cooling of thermionic thoriated tungsten cathodes under high dc-loads, Elektronenröhren u. Vakuumelektronik, NTG-Fachbericht 95, VDE-Verlag (1986), pp. 224–229
[20] G. Gaertner, NTG Fachberichte **85**, 228–232 (1983)
[21] G. Gaertner, P. Janiel, H. Lydtin, ITG Fachbericht **108**, 297–302 (1989)
[22] G. Gessinger, C. Buxbaum, High Temp.-High Press. **10**, 325–328 (1978)
[23] G. Gaertner, P. van der Heide, New Developments in CRT Cathodes, IDW 2000, Technical Digest CRT4-1, pp. 513–517
[24] G. Gaertner, D. Barratt, Appl. Surf. Sci. **251**, 73–79 (2005)
[25] B. Vancil, E. Wintucky, Appl. Surf. Sci. **251**, 101–105 (2005)
[26] Y. Wang, et al., Appl. Surf. Sci. **251**, 80–88 (2005)
[27] R. Cortenraad, A. van der Gon, H. Brongersma, G. Gaertner, A. Manenschijn, Appl. Surf. Sci. **146**, 69–74 (1999)
[28] S. Kimura, T. Higuchi, et al., Appl. Surf. Sci. **111**, 60–63 (1997)
[29] A. van Oostrom, L. Augustus, Appl. Surf. Sci. **2**(2), 173–186 (1979)
[30] S. Taguchi, T. Aida, S. Yamamoto, IEEE Trans. Electron. Devices **31**(7), 900–903 (1984)
[31] J. Hasker, J. van Esdonk, J.E. Crombeen, Appl. Surf. Sci. **26**, 173–195 (1986)
[32] J. Hasker, J.E. Crombeen, Trans. Electron. Devices **37**(12), 2589–2594 (1990)
[33] S. Yamamoto, I. Watanabe, S. Taguchi, S. Sasaki, T. Yaguchi, Jap. J. Appl. Phys. **28**, 490–494 (1989)
[34] U. van Slooten, P. Duine, Appl. Surf. Sci. **111**, 24–29 (1997)
[35] G. Gaertner, P. Janiel, J.E. Crombeen, J. Hasker, Vacuum microelectronics 1989, in IOP Conf. Ser. **99**, 25–28 (1989)
[36] G. Gaertner, P. Geittner, D. Raasch, A. Ritz, D. Wiechert, Appl. Surf. Sci. **146**, 12–16, 22–30 (1999)
[37] G. Gaertner, P. Geittner, D. Raasch, Low temperature and cold emission of Scandate cathodes, Appl. Surf. Sci. **201**, 61–68 (2002)
[38] M. Saito, et al., Higher current density oxide cathode for CRT, NTG Fachberichte **95**, 165–170 (1986)
[39] G. Gaertner, D. Raasch, D. Barratt, S. Jenkins, Accelerated life tests of CRT oxide cathodes, Appl. Surf. Sci. **215**, 72–77 (2003)
[40] G. Gaertner, P. Janiel, D. Raasch, Direct determination of electrical conductivity of oxide cathodes, Appl. Surf. Sci. **201**, 35–40 (2002)
[41] S. Hodgson, C. Goodhand, P. van der Heide, et al., Processing and performance of a novel cathode material, Appl. Surf. Sci. **146**, 79–83 (1999)
[42] T. Higuchi, Recent trends in thermionic cathodes, in *IDW'98*, CRT3-1, p. 393
[43] Y.C. Kim, K. Joo, J. Choi, H. Yang, in *IVESC 2000 Techn. Digest* D-4
[44] www.kimballphysics.com
[45] J.M. Lafferty, Boride cathodes, J. Appl. Phys. **22**(3), 299–309 (1951)
[46] H. Ahmed, A. Broers, J. Appl. Phys. **43**, 2185–2192 (1972)
[47] S. Dushman, Thermionic emission, Rev. Mod. Phys. **2**, 405–414 (1930)
[48] V. Fomenko, Emission properties of materials, NTIS, JPRS-56579 (1972)
[49] A. Makarov, et al., Cesium coated graphite emitter, Sov. Phys.-Tech. Phys. **22**(12), 1463–1465 (1978)
[50] P.A. Duine, in *IVMC*, Darmstadt, 1999, pp. 368–369
[51] P. Coates, Thermionic emission from photocathodes, J. Phys. D: Appl. Phys. **5**, 1489–1498 (1972)
[52] R.H. Good Jr., E.W. Müller, Flügge, Elektronen-Emission, in *Handbuch der Physik*, Bd. XXI (Springer, Berlin, 1956), S. 176–231

[53] R.H. Fowler, L. Nordheim, Proc. R. Soc. London Ser. A **119**, 173 (1928)
[54] E.W. Müller, Ergeb. Exakt. Naturwiss **27**, 290 (1953)
[55] K.R. Shoulders, Microelectronics using electron-beam-activated machining techniques, Adv. Comp. **2**, 135 (1961)
[56] J.W. Gewartowski, H.A. Watson, *Principles of Electron Tubes* (D. Van Norstrand, Princeton, 1965), p. 229
[57] W.P. Dyke, W.W. Dolan, *Advances in Electronics and Electron Physics*, vol. 8 (Academic, New York, 1956), p. 89
[58] C.J. Spindt, Appl. Phys. **39**, 3504 (1968)
[59] C. Spindt, I. Brodie, L. Humphrey, E.R. Westerberg, J. Appl. Phys. **47**, 5248 (1976)
[60] R. Meyer, A. Ghis, P. Ramband, F. Muller, Development of matrix array of cathode emitters on a glass substrate for flat display applications, in *Proc. 1st IVMC*, Williamsburg, VA, 1988, p. 10
[61] I. Brodie, C.A. Spindt, Appl. Surf. Sci. **2**, 149 (1979)
[62] I. Brodie, C.A. Spindt, Vacuum microelectronics, in *Advances in Electronics and Electron Physics*, ed. by P.W. Hawkes, vol. 83 (Academic, New York, 1992), p. 1
[63] D.W. Tuggle, L.W. Swanson, Emission Characteristics of the Zr-O-W thermal field electron source, J. Vac. Sci. Technol. B **3**, 220 (1985)
[64] L.W. Swanson, A comparative study of the zirconiated and build-up W cathode, J. Vac. Sci. Technol. **12**(6), 1228 (1975)
[65] H.G. König, H. Koops, A Study of Zr-O-W- and W-field emitters in an electron source at high vacuum conditions, in *Proc. Int. Conf. Microcircuit Engineering,* Berlin, 1984, ed. by A. Heuberger, H. Beneking (Academic, New York, 1985), pp. 195–202
[66] T. Asano, T. Tamon, Tech. Dig. IVMC91, 1991, p. 88
[67] M. Komuro, H. Hiroshima, J. Vac. Sci. Technol. B **9**, 2656 (1991)
[68] P.R. Schwoebel, C.A. Spindt, Appl. Phys. Lett. **63**, 33 (1993)
[69] P.R. Wilshaw, E.C. Boswell, J. Vac. Sci. Technol. B **12**, 662 (1994); M. Takai, M. Yamashita, H. Wille, S. Yura, S. Horibata, M. Ototake, Appl. Phys. Lett. **66**, 422 (1995)
[70] M. Takai, M. Yamashita, H. Wille, S. Yura, S. Horibata, M. Ototake, J. Vac. Sci. Technol. B **13**, 441 (1995)
[71] S. Matsui, K. Mori, J. Vac. Sci. Technol. B **4**, 299 (1986)
[72] H.W.P. Koops, J. Kretz, M. Rudolph, M. Weber, G. Dahm, K.L. Lee, Jpn. J. Appl. Phys. **33**, 1345 (1994)
[73] J. Kretz, M. Rudolph, M. Weber, H.W.P. Koops, Three dimensional structurization by additive lithography, analysis of deposits using TEM and EDX, and application for field emitter tips, Microelectron. Eng. **23**, 477–481 (1994)
[74] M. Takai, T. Kishimoto, M. Yamashita, H. Morimoto, S. Yura, A. Hosono, S. Okuda, S. Lipp, L. Frey, H. Ryssel, J. Vac. Sci. Technol. **14**, 1973 (1996)
[75] T. Hirano, S. Kanemaru, H. Tanoue, J. Itoh, Jap. J. Appl. Phys. **35**, 6637 (1996)
[76] K. Okano, et al., Appl. Surf. Sci. **146**, 274–279 (1999)
[77] J.F. Xu, et al., Appl. Surf. Sci. **146**, 280–286 (1999)
[78] W.B. Choi, D.S. Chung, J.H. Kang, H.Y. Kim, Y.W. Jin, I.T. Han, Y.H. Lee, J.E. Jung, N.S. Lee, G.S. Park, J.M. Kim, Appl. Phys. Lett. **75**, 3129 (1999)
[79] S.K. Kang, J.H. Choi, J.H. Park, J.-H. Han, J.-B. Yoo, J.-W. Nam, C.K. Lee, J.M. Kim, Relationship between field emission property and composition of carbon nanotube paste for large area cold cathode, J. Vac. Sci. Technol. B **22**(3), 1345 (2004)
[80] K.A. Dean, B.F. Coll, Y.W. Xie, A.A. Talin, A. Howard, C.D. Moyer, J. Trujillo, J. Jaskie, Motorola Inc. Physical Science Labs, Tempe, AZ

[81] A.G. Chakhovskoi, C.E. Hunt, G. Forsberg, T. Nilsson, P. Persson, Reticulated vitreous carbon field emission cathodes for light source applications, J. Vac. Sci. Technol. B **21**, 571 (2003)
[82] H. Busta, Field emission flat panel displays, Chapter 7, in *Vacuum Microelectronics*, ed. by W. Zhu (Wiley, New York, 2001)
[83] E.A. Hijzen, The avalanche cold cathode for CRTs, in *IDW'98*, 1998, pp. 405–408
[84] A.M.E. Hoebrechts, G.G.P. van Gorkum, Design, technology, and behavior of a silicon avalanche cathode, J. Vac. Sci. Technol. B **4**, 105 (1986)
[85] S.H. Jo, J.D. Lee, Fabrication and analysis of a silicon tip avalanche cathode, J. Vac. Sci. Technol. B **13**(2), 469 (1995)
[86] W. Fuhs, P. Kanschat, K. Lips, Bandtails and defects in microcrystalline silicon (mu c-Si:H), J. Vac. Sci. Technol. B **18**, 1792 (2000)
[87] J.-S. Kim, T. Hoshi, K. Sawada, M. Ishida, Planar metal–insulator–semiconductor type field emitter fabricated on an epitaxial Al/Al2O3/Si (111) structure, J. Vac. Sci. Technol. B **22**, 1358–1361 (2004)
[88] H.A. Baba, T. Yoshida, T. Asano, Field emission characteristics of defect-controlled polyimide tunnelling cathode, J. Vac. Sci. Technol. B **22**, 1353–1357 (2004)
[89] Riege, Ferroelectric electron emission: Principles and technology, Appl. Surf. Sci. **111**, 318–324 (1997)
[90] J.D. Clewley, A.D. Crowell, D.W. Juenker, Changes in photoelectron emission from molybdenum due to exposure to gases, J. Vac. Sci. Technol. **9**, 877 (1972)
[91] T.E. Fischer, Photoemission and surfaces, J. Vac. Sci. Technol. **9**, 860 (1972)
[92] http://www.saesgetters.com
[93] D. Martin, et al., Design of glass substrates and spacers for FEDs, Saint-Gobain Display Glass, France, Technical digest EURO FE, 2002
[94] http://www.mems-exchange.org/catalog/
[95] J. Dziuban, R. Walczak, Microwave enhanced wet anisotropic etching of silicon utilizing a memory effect of KOH activation – a remote E2MSi process, in *The 16th European Conference on Solid-State Transducers Eurosensors XVI*, Prague, Czech Republic, T1A3, September 15–18, 2002
[96] J. Eichmeier, *Moderne Vakuumelektronik* (Springer, Berlin, 1981), chapter 9.4
[97] J. Eichmeier, H. Heynisch (ed.), *Handbuch der Vakuum-elektronik* (R. Oldenbourg, München, Wien, 1989), chapter 2
[98] W. Kohl, *Handbook of Materials and Techniques for Vacuum Devices* (Reinhold Publishing corporation, 1967)